

Contents

| | |
|--|----------|
| 1 A Physicist's Map of Human Opinions | 1 |
| 1.1 Society as a Multi-Scale Complex System | 1 |
| 1.2 Opinion Formation: Emergent Patterns of Social Interaction | 2 |
| 1.2.1 Models of Opinion Dynamics and Polarization | 3 |
| 1.2.2 Addressing Polarization and Echo Chambers | 4 |
| 1.3 Electoral Processes: Critical Events in Collective Decision-Making | 5 |
| 1.3.1 The Search for Universal Patterns in Electoral Data | 6 |
| 1.3.2 Margins of Victory and Voter Turnout | 6 |
| 1.4 Structural Overview and Research Framework | 7 |
| 2 A Gentle Nudge Against Online Polarization | 9 |
| 2.1 Opinion Dynamics in Digital Social Networks | 9 |
| 2.2 Theoretical Framework: A Model of Opinion Dynamics | 10 |
| 2.2.1 The Opinion Dynamics Framework | 10 |
| 2.2.2 The Three States of Opinion Dynamics | 12 |
| 2.2.3 Quantitative Metrics for Polarization Assessmen | 13 |
| 2.3 The Intervention: The “Random Nudge” Strategy | 14 |
| 2.3.1 Mechanisms and Challenges of Echo Chamber Formation | 15 |
| 2.3.2 The Random Nudge Mechanism | 15 |
| 2.3.3 Mathematical Formulation | 16 |
| 2.4 Empirical Results of the Random Nudge Intervention | 16 |
| 2.4.1 Depolarization Effects | 16 |
| 2.4.2 Network Effect: Breaking of Distinct Clusters | 17 |
| 2.4.3 Quantitative Analysis of Polarization Reduction | 19 |
| 2.5 Balancing Depolarization Against Radicalization Risk | 20 |
| 2.5.1 Finding the Sweet Spot: Optimizing the Nudge | 21 |

CONTENTS

| | | |
|----------|---|-----------|
| 2.6 | Robustness Check: Testing on Alternative Models | 22 |
| 2.7 | Discussion and Implications | 23 |
| 2.7.1 | Implications for Digital Platform Design | 24 |
| 2.7.2 | Ethical Considerations and Implementation Challenges | 24 |
| 2.7.3 | Broader Implications for Collective Decision-Making | 24 |
| 3 | Digging into the Data: The Foundation of Electoral Analysis | 28 |
| 3.1 | The Pivot: From Opinions to Elections | 28 |
| 3.2 | Data Collection Methodology and Sources | 28 |
| 3.3 | Dataset Structure and Variable Definitions | 29 |
| 3.4 | Data Processing and Quality Assurance | 30 |
| 3.5 | Descriptive Statistics and Cross-National Patterns | 31 |
| 3.6 | Dataset Validation and Analytical Framework | 34 |
| 4 | Universal Clues in the Ballot Box | 36 |
| 4.1 | The Quest for Electoral Universality: From Previous Attempts to New Approaches | 36 |
| 4.1.1 | Historical Approaches to Electoral Universality: Prior Research and Limitations | 36 |
| 4.1.2 | Exploring Universality in the Electoral Competition | 37 |
| 4.2 | The Electoral Process: A Template | 37 |
| 4.2.1 | The Dance of Turnout and Margin | 38 |
| 4.2.2 | The Need for a Scale-Independent Measure | 40 |
| 4.3 | The Specific Margin: A Scale-Invariant Approach | 41 |
| 4.3.1 | Universal Distribution of Scaled Specific Margin | 41 |
| 4.4 | Theoretical Challenges in Explaining Statistical Universality | 43 |
| 4.4.1 | A Glimpse of the Mechanism: The Random Voting Model | 43 |
| 4.5 | Conclusion: Universality as a Signature of Democratic Competition | 45 |
| 5 | The Random Voting Model: When Chance Explains Choice | 48 |
| 5.1 | Introducing the Random Voting Model (RVM): Simplicity by Design | 48 |
| 5.2 | Analytical Derivation of the Universal Specific Margin Distribution | 49 |
| 5.2.1 | The Set-up: Large Turnout Limit | 50 |
| 5.2.2 | Order Statistics: The Key to Understand Ranking | 50 |
| 5.2.3 | Application to the Random Voting Model | 51 |
| 5.3 | Predicting Margin Distributions from Turnout Distributions | 53 |

| | | |
|-------------------|--|-----------|
| 5.3.1 | Turnout Distribution Effects on Margin Distribution | 53 |
| 5.3.1.1 | Exponential Turnout Distribution | 53 |
| 5.3.1.2 | Power law Turnout Distribution | 54 |
| 5.3.1.3 | Gaussian Turnout Distribution | 55 |
| 5.3.1.4 | Uniform Turnout Distribution | 55 |
| 5.3.2 | RVM Simulations with Synthetic Turnout Distributions | 56 |
| 5.3.3 | The Necessity of Scaling in Margin Distribution Analysis | 58 |
| 5.3.3.1 | Predicting Scaled Margin Distributions Across Countries . . . | 58 |
| 5.3.3.2 | Scale-Independent Predictive Accuracy | 59 |
| 5.3.3.3 | Comprehensive Validation Across All Countries | 59 |
| 5.4 | Conclusion: The Power and Limitations of RVM | 61 |
| 6 | Beyond Margins: Winner and Runner-up votes | 63 |
| 6.1 | The Effective Number of Candidates | 63 |
| 6.2 | Relationship Between Turnout and Vote Distributions | 64 |
| 6.3 | Predicting Vote Distributions from Turnout Distributions | 65 |
| 6.3.1 | Random Voting Model: a Quick Recap | 66 |
| 6.3.2 | Vote Share Distributions at Large Turnout Limit | 66 |
| 6.3.3 | Random Voting Model with two candidates | 66 |
| 6.3.3.1 | Winner vote share distribution | 67 |
| 6.3.3.2 | Runner-up vote share distribution | 67 |
| 6.3.4 | Random Voting Model with three candidates | 68 |
| 6.3.4.1 | Winner vote share distribution | 68 |
| 6.3.4.2 | Runner-up vote share distribution | 69 |
| 6.3.5 | Calculating the <i>scaled</i> distributions | 69 |
| 6.4 | Empirical Validation across Electoral Scales | 70 |
| 6.5 | Scale Invariance of Margin Distributions in Indian Elections | 72 |
| 6.6 | Conclusion: Turnout Distributions as Electoral Predictors | 74 |
| References | | 77 |

CHAPTER 1

A Physicist’s Map of Human Opinions

Society represents one of nature’s most intricate complex systems—a vast ensemble of interacting individuals whose collective behaviors emerge across multiple scales, from ephemeral digital trends to enduring democratic institutions. The emergent properties arising from these interactions often manifest as non-trivial macroscopic patterns that cannot be easily inferred from individual behaviors [1]. Much like how individual water molecules give rise to the unexpected phenomenon of waves, individual human decisions combine to create societal patterns that no single interaction could predict. This thesis employs the tools of statistical physics to investigate two fundamental aspects of collective human behavior: opinion formation in digital networks and universal patterns in democratic elections. Through this examination, we demonstrate that randomness, properly understood and harnessed, serves as both an explanatory principle and a constructive force for understanding and improving social systems.

1.1 Society as a Multi-Scale Complex System

Human society operates across extraordinarily diverse scales, both spatial and temporal. Spatially, interactions span from local communities to global networks, encompassing physical proximity interactions and increasingly, technology-mediated connections that transcend geographic constraints [2]. Temporally, processes range from millisecond-scale information transmission to decade-spanning political movements and generational cultural shifts. This multi-scale nature creates layered feedback mechanisms that make social systems resistant to reductionist analysis.

Consider how a single tweet can trigger cascading reactions across millions of users within minutes, while simultaneously contributing to slowly-evolving cultural narratives that unfold over years. These cross-scale interactions create feedback loops where macro-level structures shape individual behaviors, which in turn reshape those very structures—a dynamic reminiscent of how atoms collectively determine the properties of materials which then constrain atomic movement.

Within this complex landscape, opinion formation and electoral processes represent critical mechanisms through which individuals collectively navigate their shared environment. These

processes share common features with physical systems that have long been studied using statistical mechanics—they involve numerous interacting components, exhibit emergent behaviors, and often display robust statistical regularities despite their apparent complexity [3, 4]. However, they also present unique challenges: human agents possess agency, adaptability, and strategic behavior absent in physical particles.

The statistical physics approach to social dynamics leverages powerful analytical tools developed for understanding physical systems while acknowledging these distinctive features of social interactions. This approach focuses not on predicting individual behavior but on identifying statistical patterns that emerge at the population level, along with the mechanisms that generate them. The value of such an approach lies in its ability to abstract away unnecessary details while preserving essential dynamics that govern system behavior.

1.2 Opinion Formation: Emergent Patterns of Social Interaction

Opinions do not exist as static, independent properties of individuals but rather as dynamic outcomes of complex social interactions. These interactions are increasingly mediated by digital technologies that reshape the fundamental processes of information diffusion and opinion formation [2]. Online platforms now serve as primary arenas where individuals encounter information, form judgments, and express beliefs on topics ranging from trivial consumer choices to consequential political positions.

Much as stars form nebulae through their gravitational pull on surrounding matter, influential voices and trending topics create opinion clusters that shape the broader information landscape. These nebulae of opinion are not fixed—they expand, contract, split, and merge as new information enters the system and social connections evolve.

The information revolution has lowered the entry barrier for nearly everyone to participate and contribute to shaping opinions and policies on various issues. This has been largely aided by the easy availability of social media infrastructure through mobile devices. Increasingly, the collective opinions expressed through various social media platforms are thought to be one barometer of the public mood on any contentious issue of the day [2]. This provides an interesting testing ground for the dynamics and statistical physics of interacting multi-agent systems since the online nature of interactions provides fine-grained data for quantitative analysis and comparison with model results.

Recent empirical studies have documented concerning trends in these digital opinion landscapes. Controversial issues consistently display bimodal opinion distributions, indicating polarization rather than consensus [5–7]. This polarization is often reinforced through homophilic interactions—individuals preferentially engaging with others holding similar views—creating what researchers term “echo chambers” [8–12]. Platform recommendation algorithms, optimized for user engagement, frequently amplify these natural homophilic tendencies, potentially accelerating polarization processes [13].

1.2.1 Models of Opinion Dynamics and Polarization

The study of opinion formation and its dynamics has attracted researchers for decades. The analysis of opinion dynamics from the statistical physics perspective can be traced back to the work of DeGroot [14], which provides a framework for reaching a consensus. Several models, including the voter model [15, 16], Sznajd model [17, 18], and their variants which have a strong basis in a framework of interacting spins, suggest that large participatory interactions among agents might also lead to the emergence of consensus.

At their core, these models capture a fundamental insight: opinions change through social influence. When individuals interact, their views tend to shift based on those they encounter—much like how particles exchange energy upon collision. The simplest models assume a straightforward convergence process, where repeated interactions lead to a gradual alignment of views across the population.

However, empirical results have shown that the distribution of opinions tends to show a bimodal distribution pattern corresponding to polarization, especially on controversial issues of the day [5–7]. Culture dissemination model [19], one of the first higher-dimensional modeling approaches to opinion dynamics, which also incorporates the human tendency to interact with similar persons, shows that despite there being local convergence, global polarization can be reached.

Other discrete models by Galam et al. [1, 3, 4, 20] explain the effects of consensus, attitude changes in groups, and the spreading of minority opinions. In the presence of stubborn agents, these models can also capture the effect of polarization [21–23]. Different variants of the bounded confidence model [24, 25] can also capture many empirically found trends in the distribution of opinions. These models can reproduce consensus, bimodal, or multi-modal opinion distributions depending on the confidence interval.

More recent models have incorporated homophily and algorithmic feedback effects, successfully reproducing the emergence of polarized states and echo chambers. Among these, the model by Baumann et al. [26] demonstrates particular empirical fidelity, capturing key features of digital polarization including active extremists, opinion clusters, and reinforcement mechanisms.

Traditional opinion dynamics models from statistical physics typically predict convergence toward consensus under broad conditions. These models fail to capture the persistent polarization observed empirically. Recent empirical evidence for echo chamber effects has been reported from several social media platforms [9–12]. Few recent opinion dynamics models [13, 26–28] have qualitatively captured the features of echo chambers, which have been shown to arise from personalized interactions among peers in an online setting, which might be accelerated through the platform’s recommendation engine.

1.2.2 Addressing Polarization and Echo Chambers

Though having diverse opinions might be a desired outcome, extreme polarization leads to network segregation [29], which often bottlenecks the information flow in social networks. At an individual level, people in highly polarized environments experience reduced exposure to diverse perspectives, and at a societal level, this fragmentation can undermine the shared factual basis necessary for collective decision-making.

Echo chambers, often linked to polarization, are known to be responsible for sustaining misinformation for a longer time on social networks [30, 31]. Think of echo chambers as information cul-de-sacs, where ideas circulate but rarely exit—creating closed loops that resist correction or evolution. As individuals become increasingly isolated in these self-reinforcing information environments, their resistance to contradictory information grows, making depolarization increasingly difficult.

These problems call for intervention mechanisms, which should be safe and non-invasive. Just as a physicist might introduce a controlled perturbation to study or alter a physical system’s behavior, we can consider strategic interventions in digital networks to reduce harmful polarization without compromising individual agency.

It might appear that in the case of controversial topics, the interaction and debate will always lead to polarized states of opinion. But the underlying mechanism for polarization—the reinforcement of opinions through interaction between like-minded people—leaves us wondering if any intervention will help to reconcile disparate opinions.

Understanding and potentially mitigating digital polarization presents both theoretical and practical challenges. Any intervention must balance multiple objectives: reducing polarization without promoting radicalization, preserving user engagement, and respecting individual privacy. Additionally, defining a “healthy” opinion distribution is itself normatively complex, requiring careful consideration of democratic values and information ecosystem diversity.

Echo chambers are increasingly becoming more apparent in online social media platforms. A generic tendency to interact with people who hold similar opinions as ours can lead to echo chambers, and this effect is, in turn, amplified by the recommendation engines on social media platforms. These algorithmically driven engines recommend similar connections or content in order to keep the users of those platforms engaged.

1.3 Electoral Processes: Critical Events in Collective Decision-Making

Electoral processes represent a formalized mechanism through which individual preferences aggregate to produce collective decisions. If everyday opinion formation resembles the slow accretion of nebulae, elections are like supernovae—intense, concentrated events where the energy of millions of individual choices release their power in a single moment, potentially altering the landscape of governance.

Elections, the cornerstone of democratic societies, are usually regarded as unpredictable due to the complex interactions that shape them at different levels. Democratic elections constitute some of the most extensively documented instances of large-scale collective human behavior, with records spanning decades and encompassing hundreds of millions of voters.

One of the cornerstones of democratic societies is that governance must be based on an expression of the collective will of the citizens. The institution of elections is central to the operational success of this system. Elections to public offices are the best-documented instances of collective decision-making by humans, whose outcome is determined by multiple agents interacting over a range of spatial and temporal scales. These features make elections an interesting test-bed for statistical physics whose key lesson is that a multitude of complex interactions between microscopic units of a system can manifest into robust, *universal* behavior at a macroscopic level [32–44]. A collection of gas molecules or spins are examples that display such emergent macroscopic features [45], and so are complex processes such as earthquakes [46, 47] and financial markets [48]. In the context of elections, such universal behaviors serve to distill the complexities of electoral

dynamics into understandable and predictive frameworks and safeguard its integrity.

1.3.1 The Search for Universal Patterns in Electoral Data

Unsurprisingly, the possibility of universality in elections attracts significant research attention [49–55]. Several works have studied and proposed models for (*a*) the distribution $q(\sigma)$ of the fraction of votes σ obtained by candidates (or the vote share), and (*b*) distribution $g(\tau)$ of voter turnout τ . While σ is indicative of popularity, τ indicates the scale of the election. Though some universality has been observed in $q(\sigma)$ or $g(\tau)$ within a single country [49–51] or in countries with similar election protocols [50, 54], deviations from claimed universalities have also been reported [54, 56–59] due to variations in the size (scale) of electoral districts and weak party associations.

Though voting patterns tend to display spatial correlations [60–63], it is not known to be universal. Despite the availability of enormous election data and persistent attempts, a robust and universal emergent behavior, valid across different scales and countries with vastly different election protocols, is yet to be demonstrated. This absence of truly robust universality across different countries and electoral scales has remained a significant gap in our understanding of collective voting behavior.

1.3.2 Margins of Victory and Voter Turnout

Among the many statistics of interest, the *margin* of victory, defined as the difference between votes for the winner and runner-up candidates, encodes key information about the competitiveness of elections. While margins of victory have been previously studied [64–69], often independently of voter turnouts.

However, our empirical analysis using extensive election data [70–73] from 34 countries (from 6 continents) spanning multiple decades and electorate scales, shows that margins of victory are strongly correlated with voter turnout and can be leveraged to demonstrate a robust universality. By examining how these quantities scale with each other, we uncover patterns analogous to scaling laws in physical systems—where relationships between variables remain consistent across different scales of observation.

The significance of such findings extends beyond academic interest. Understanding the statistical properties of electoral competition can provide baselines for detecting anomalies that might indicate manipulation [74–80] inform electoral system design, and shed light on the fundamental nature of democratic competitions.

1.4 Structural Overview and Research Framework

The thesis proceeds through several interlinked investigations, each reinforcing a unified theme: leveraging randomness constructively to decode and enhance social systems:

Chapter 2 introduces and optimizes the “random nudge” intervention strategy against digital polarization. Building on our understanding of opinion dynamics, we demonstrate how carefully calibrated random interventions can counteract the reinforcement mechanisms that drive polarization without compromising system integrity.

Chapter 3 details extensive data collection and curation efforts, laying the empirical foundation for electoral analysis. This chapter bridges theory with real-world observation, establishing the robust dataset necessary for testing universal patterns.

Chapter 4 explores and empirically validates the universality in scaled margin-to-turnout ratios across multiple electoral systems. We demonstrate how properly normalized electoral statistics reveal striking patterns across diverse democratic contexts.

Chapter 5 develops the Random Voting Model (RVM), analytically deriving and validating predictions against extensive electoral data. This model demonstrates how stochastic processes, properly understood, can capture essential features of complex social decision-making.

Chapter 6 further explores the Random Voting Model to predict several other key electoral statistics, with a focus on the Indian context. This extends our theoretical framework to additional empirical tests, strengthening the potential of the model.

Chapter 7 demonstrates some practical applications, from intervention design to detecting electoral malpractices. Here, we translate theoretical insights into pragmatic tools for improving social systems.

Chapter 8 provides a comprehensive discussion synthesizing our findings across both opinion dynamics and electoral patterns, offering broader implications and future research directions.

Having established the foundational context, we now embark on our first critical inquiry—designing an effective intervention to mitigate online polarization through strategic randomness.

CHAPTER 2

A Gentle Nudge Against Online Polarization

In the previous chapter, we established the motivation for understanding complex societal phenomena through the lens of statistical physics. We now shift our focus towards a specific challenge of the digital age: the polarization of opinions in online social networks. In this chapter, we will introduce and analyze a novel intervention strategy - the “random nudge” - that can effectively reduce polarization without causing undesirable side effects.

2.1 Opinion Dynamics in Digital Social Networks

Having examined the broader landscape of opinion formation in Chapter 1, we now focus on developing tangible solutions to the polarization challenge. As previously established, the empirically observed bimodal opinion distributions and the formation of echo chambers represent significant challenges in modern digital environments. These patterns resist the consensus predictions of traditional opinion dynamics models and create self-reinforcing information silos that impede healthy discourse.

Building on the foundation of existing models, we will adapt a recently introduced framework that successfully captures key empirical features of online opinion dynamics, including polarization, echo chambers, and the tendency for more active users to hold stronger opinions. This model provides an ideal testbed for exploring intervention strategies aimed at reducing harmful polarization.

The central question we address is whether a minimal intervention can effectively disrupt the reinforcement cycles that drive polarization without compromising individual agency or platform engagement. Specifically, we will demonstrate that a carefully calibrated “random nudge” can achieve substantial depolarization while avoiding the pitfalls of radicalization.

While Chapter 1 provided a comprehensive review of opinion dynamics models, we’ll focus here on the specific framework that will enable us to test our intervention strategies. Of particular relevance is the model introduced by Baumann et al. [26], which successfully captures key empirical features observed in online social networks: polarized opinion distributions, echo chamber

formation, and the tendency for more active users to hold more extreme opinions. This model demonstrates how homophilic interactions—the preference to connect with those holding similar opinions—naturally lead to polarized states even from initially diverse opinion distributions.

Our intervention approach is motivated by the underlying mechanism of polarization: the reinforcement of opinions through homophilic interactions. We hypothesize that by strategically disrupting this reinforcement cycle, we can achieve depolarization. Specifically, we introduce a “random nudge” intervention that exposes agents to more diverse opinions. Through simulation and analysis, we will demonstrate that this approach can effectively break echo chambers when calibrated appropriately.

However, our findings also reveal an important caution: excessive intervention can lead to radicalization [81, 82]—a state where all agents adopt the same stance on an issue. This creates a delicate optimization problem: finding the precise intervention strength that reduces polarization without triggering radicalization. We will formulate and solve this optimization problem to compute the optimal nudge parameters for achieving a healthier opinion distribution.

2.2 Theoretical Framework: A Model of Opinion Dynamics

Having identified our approach, we now provide a detailed mathematical formulation of the opinion dynamics model that will serve as our experimental testbed. We adapt the framework introduced by Baumann et al. [26], which allows us to rigorously analyze how interventions affect the evolution of opinions in digital social networks.

2.2.1 The Opinion Dynamics Framework

The model has N interacting agents, and it is assumed there are only two possible sides to an issue. This is typical of many, but not all, the issues – for example, to allow abortion or not. Opinion on a given issue is denoted by x_i , which can take any real value in the range $(-\infty, \infty)$. The sign of the x_i corresponds to the stance of the agent in the corresponding issue, and $|x_i|$ denotes the conviction of the agent in their respective stance. This implies that the larger the value of $|x_i|$, the more extreme the agent’s opinion is.

The model used to capture the evolution of opinion is activity driven [83–86], *i.e.*, at each time step, only active agents are can influence other agents. Based on empirical data [83, 85], the

distribution of agent's activity chosen to be,

$$F(a) = \frac{1 - \gamma}{1 - \varepsilon^{1-\gamma}} a^{-\gamma}, \quad (2.1)$$

where a is the activity, ε is the minimum activity (chosen in this work to be 10^{-2}), and γ controls how steep the function $F(a)$ which is chosen to be 2.1.

In simpler terms, this activity distribution means that most agents have low activity levels (they rarely post or interact), while a few agents are highly active (frequent posters) – similar to what we observe in real social media platforms where a small percentage of users generate the majority of content.

Agents' opinions evolve based on their interactions with other agents, and this information is encoded in the time-dependent adjacency matrix $A_{i,j}(t)$. Further, opinion evolution also depends on the strength of social interaction $K > 0$ and the controversialness of the issue $\alpha > 0$. The opinion dynamics is given by the following N coupled differential equations [26]

$$\dot{x}_i = -x_i + K \left(\sum_{j=1}^N A_{ij}(t) \tanh(\alpha x_j) \right). \quad (2.2)$$

To understand this equation intuitively: an agent's opinion (x_i) changes based on two opposing forces – a natural tendency to moderate their view over time (the $-x_i$ term), and the influence from other agents they interact with (the sum term). The parameter K determines how much weight social influence has compared to the natural moderation tendency. While people with extreme opinions have stronger influence than moderately opinionated ones, the tanh function ensures the social influence of each person is limited between -1 and 1 .

In this, $A_{i,j}(t)$ is the temporal adjacency matrix of interaction at time t . If at time t agent j influences agent i , than $A_{i,j}(t) = 1$, and $A_{i,j}(t) = 0$ otherwise. If agent i is active at time t , they will interact with m other agents, weighted by the probability $P_{i,j}$.

Further, the probabilistic reciprocity factor $r \in [0, 1]$ determines the chance that an interaction is mutually influential, *i.e.*, $A_{ij}(t) = A_{ji}(t) = 1$. The interaction probability is defined to be a function of the magnitude between two agents' opinions.

$$P_{ij} = \frac{|x_i - x_j|^{-\beta}}{\sum_k |x_i - x_k|^{-\beta}}, \quad (2.3)$$

where β is the homophily factor which quantifies the tendency for agents with similar opinions to interact with each other: $\beta = 0$ refers to the absence of interaction preference, and $\beta > 0$ implies

that the agents with similar opinions are more likely to interact with one another. Evidently, Eq. (2.3) is modeled as a power-law decay of connection probabilities with only a small chance for agents with opposite opinions to interact. Since most of the interactions tend to occur between agents with similar opinions, this can lead to the formation of echo chambers.

This homophily equation captures the tendency we observe in real life: people prefer to interact with those who share similar opinions. The higher the β value, the stronger this tendency – representing how we might naturally gravitate toward content and people who reinforce our existing views, creating “filter bubbles” or echo chambers.

2.2.2 The Three States of Opinion Dynamics

Now that we have established the mathematical foundation of our model, we can examine the emergent collective behaviors that arise from these individual interactions. Depending on the strength of social interaction (K) and the homophily factor (β), the model exhibits three distinct steady states that closely resemble opinion distributions observed in real-world scenarios.

The interaction dynamics in the model is enforced by the activity-driven temporal network that is fully encoded by the parameters $(\varepsilon, \gamma, m, \beta, r)$, together with the parameters that characterise the issue, (K, α) . Asymptotically, this model features three distinct states in the distribution of opinions. If the Social interaction K is sufficiently small, then the opinion of every agent decays to zero, and this state is known as the neutral consensus state. However, if social interaction K is large but the homophily factor β is small, then due to statistical fluctuations, all the opinions either become positive or negative. This state, where each agent has the same stance (the sign of x_i for all i is the same) with possibly different convictions, is called radicalization. It is important to note that radicalization is an absorbing state of this model. This is because when all agents have opinions with the same sign, the dynamics does not allow for a sign-change of any agent’s opinion. The most interesting case emerges when social interaction K and homophily factor β are large enough. In this case, a meta-stable polarized state emerges, which is characterized by a bimodal opinion distribution.

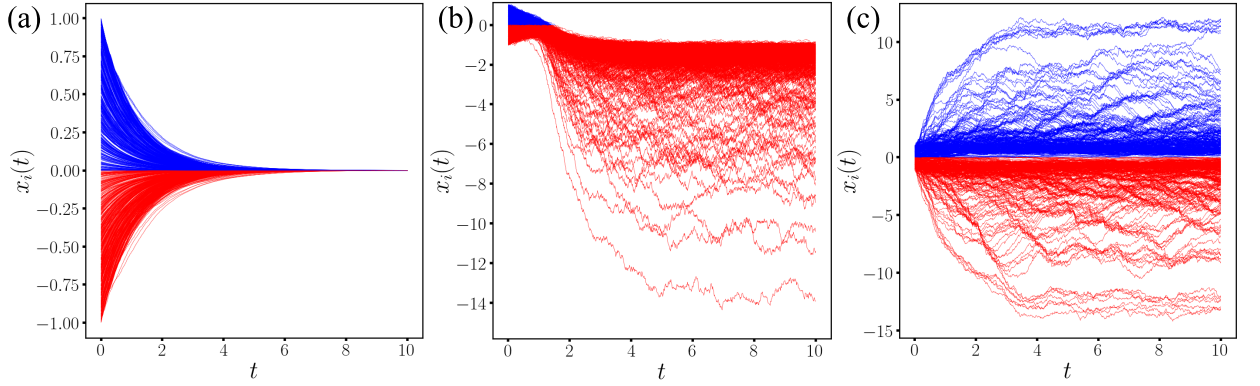


Figure 2.1: A schematic illustrating the three fundamental states of opinion dynamics. Panel (a): The consensus state, characterized by all agents converging to neutral opinions (near zero) in the absence of strong social interaction. Panel (b): The radicalization state, where all agents adopt the same stance (either all positive or all negative opinions) with varying degrees of conviction. Panel (c): The polarized state, featuring a bimodal opinion distribution where the population splits into two opposing groups, creating the familiar “two peaks” pattern often observed in controversial social issues.

2.2.3 Quantitative Metrics for Polarization Assessment

Before we delve into the details of the intervention strategy and results, we discuss the three quantities employed to measure the degree of polarization based on the opinion distribution $P(x)$. They are defined as: (a) Polarization is measured through $\bar{\Delta}$, defined as the distance between the average of positive opinions and the average of negative opinions. b) When opinion distribution exhibits a bimodal character, the distance between the two peaks, denoted by Δ_{peak} , can also be used as a measure of polarization [87]. (c) A gross measure of polarization could also be the standard deviation σ of the entire opinion distribution [13]. Fig. 2.2 illustrates the schematics of all three measures of polarization. It must be noted that if polarization decreases due to the intervention proposed in Eq. (2.4), ideally, all these three quantifiers must decrease.

These measures have practical applications in analyzing real-world opinion data. For example, $\bar{\Delta}$ can be calculated from survey data where respondents rate their agreement with statements on a numerical scale. In social media analysis, Δ_{peak} might be observed in the distribution of sentiment scores on controversial topics, where comment sentiment often clusters around two opposing positions. The standard deviation σ is particularly useful when analyzing large-scale data from platforms like Twitter or Reddit, where the full spectrum of opinions can be mapped and quantified.

Importantly, these metrics capture complementary aspects of polarization. $\bar{\Delta}$ focuses on the

”distance” between opposing groups, Δ_{peak} highlights the most prominent opinion clusters, while σ measures the overall spread regardless of modality. By tracking all three simultaneously, we can distinguish between different types of opinion shifts—for instance, distinguishing between genuine depolarization versus a shift where opinions remain far apart but become less concentrated around specific values.

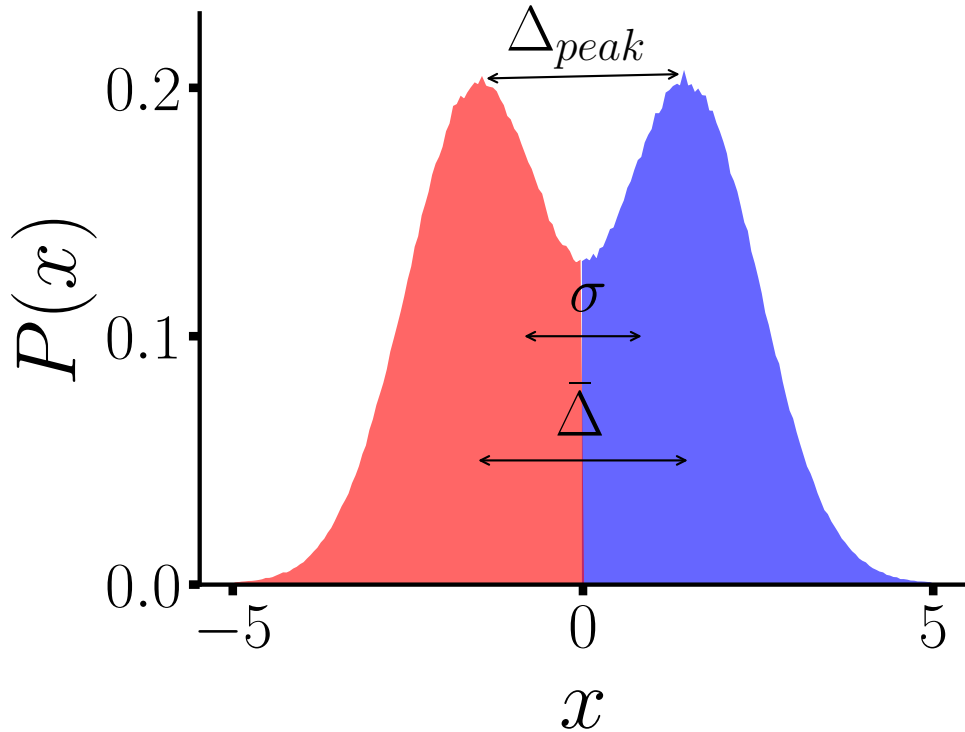


Figure 2.2: Schematic illustration of three complementary measures of polarization used in this study. $\bar{\Delta}$ (left) represents the distance between mean positive and negative opinions, capturing the average separation between opposing groups. Δ_{peak} (center) measures the distance between the two peaks in a bimodal opinion distribution, highlighting the gap between the most common opposing viewpoints. σ (right) denotes the standard deviation of the entire opinion distribution, quantifying the overall spread of opinions across the population. All three metrics decrease when polarization is successfully reduced.

2.3 The Intervention: The “Random Nudge” Strategy

Having established the model dynamics and identified how polarization emerges and can be measured, we now turn our attention to a key question: How can we effectively counter the formation of echo chambers and reduce polarization in online social networks?

2.3.1 Mechanisms and Challenges of Echo Chamber Formation

Echo chambers are increasingly becoming more apparent in online social media platforms. These self-reinforcing information environments arise from two primary mechanisms:

- First, there is our natural tendency toward homophily—we prefer to interact with people who hold similar opinions to our own. In our model, this is captured by the homophily factor β , where larger values represent more closed and isolated echo chambers.
- Second, this natural tendency is often amplified by recommendation engines on social media platforms. These algorithmically driven systems recommend similar connections or content to keep users engaged, inadvertently strengthening opinion bubbles.

The challenge lies in developing interventions that can effectively disrupt these echo chambers while simultaneously maintaining user engagement on the platforms and respecting user privacy and preferences. Such interventions should ideally not require knowledge of users’ specific opinions and should create sustainable diversity rather than just temporary exposure to different viewpoints. This is a delicate balance to achieve in practice.

2.3.2 The Random Nudge Mechanism

To address these challenges, we propose a simple yet powerful intervention strategy — the “random nudge.” The core principle is introducing a controlled amount of randomness into user interactions:

With probability p (where $p < 1$), active agents will interact uniformly with any other agents in the network, regardless of opinion similarity. With the complementary probability $(1 - p)$, interactions proceed according to the normal homophily-based probability given in Eq. (2.3).

This approach offers several advantages over more direct interventions. It preserves privacy since it requires no knowledge of agent opinions or beliefs. The intervention strength can be precisely controlled by adjusting the parameter p , allowing for fine-tuning based on the specific context. Additionally, it maintains the platform’s engagement-driven structure while introducing just enough diversity to prevent echo chamber formation. Perhaps most importantly, it creates natural opportunities for cross-opinion exposure without forcing specific content on users, which could lead to disengagement or reactance.

2.3.3 Mathematical Formulation

We implement this random nudge by modifying the interaction probability as follows:

$$\tilde{P}_{ij} = p \times \frac{1}{N-1} + (1-p) \times P_{ij}. \quad (2.4)$$

The first term represents the uniform random interaction (each agent has equal probability $\frac{1}{N-1}$ of interacting with any other agent), while the second term preserves the homophily-driven interactions proportional to the original P_{ij} . The parameter p controls the strength of the intervention—higher values introduce more randomness, while values closer to zero preserve more of the natural homophily-driven structure.

This modified interaction probability is used for all subsequent simulations presented in this chapter. As we will demonstrate, even small values of p can lead to dramatic reductions in polarization and the breakdown of echo chambers.

2.4 Empirical Results of the Random Nudge Intervention

With the intervention strategy introduced in Sec. 2.3, we find that with sufficiently small random nudge probability p , significant depolarization can be obtained, which is evident as the opinion distributions approach towards a unimodal distribution along with the decay of all three measures of polarization. To see the effects of nudge, we perform numerical simulations of the basic model in Eq. (2.2) using the interaction probability given in Eq. (2.3) and the intervention model in Eq. (2.4). The simulations are performed with $N = 5000$ agents for 1000 time steps with $dt = 0.01$. At initial time x_i is uniformly chosen from a small interval, *i.e.*, $x_i \in [-1, 1]$ for $i = 1, 2 \dots N$. The model parameters are chosen to be $\alpha = 3$, $\beta = 3$, $K = 3$, $m = 10$, $\gamma = 2.1$, $\varepsilon = 0.01$ and $r = 0.5$ for all the simulations unless mentioned otherwise. The parameters chosen for the simulations lead to a polarized state in the original model without intervention. Our analysis reveals several key insights into how small perturbations can lead to significant changes in collective behavior patterns.

2.4.1 Depolarization Effects

In Fig. 2.3, we show the contrast between the trajectories of individual opinions and the opinion distribution with and without the application of a nudge. In the absence of nudge ($p = 0$), the simulation results in Fig. 2.3(a) show fewer trajectories with opinions $x_i \approx 0$. This leads to a

bimodal distribution of opinions characteristic of a polarized state. In contrast, in Fig. 2.3(b), a small nudge with a probability of $p = 0.01$ is applied, and we find significantly more trajectories with moderate opinions. This, effectively, is seen to lead to an absence of polarization, which is evident from the unimodal opinion distribution. The magnifications of the region around $x_i = 0$ and its distribution (shown in Fig. 2.3) reveal a clear distinction between these two scenarios.

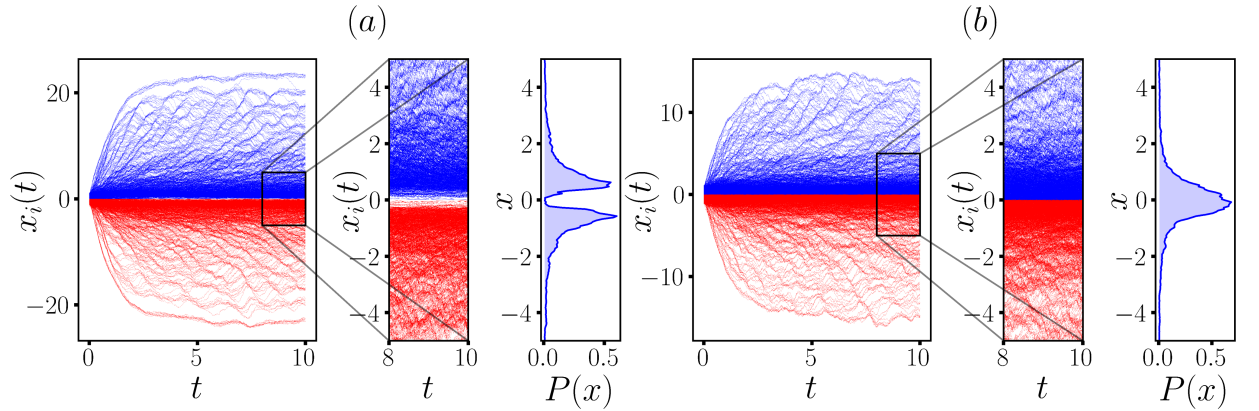


Figure 2.3: Visualization of opinion trajectories and resulting distributions with and without the random nudge intervention. (a) Without nudge ($p = 0$): Opinion trajectories show clear divergence, avoiding the moderate region around $x = 0$ (shown in the magnification). The resulting distribution (right panel) is distinctly bimodal, indicating strong polarization with few moderate opinions. (b) With a small nudge ($p = 0.01$): Opinion trajectories show significant crowding around $x = 0$ (magnification), leading to a nearly unimodal symmetric distribution (right panel). This demonstrates how even a minimal random intervention can substantially reduce polarization by promoting moderate viewpoints.

2.4.2 Network Effect: Breaking of Distinct Clusters

To examine the effect of network nudge, we analyze the underlying time-averaged structures of the temporal interactions network. Without nudge, the interaction network has two distinct clusters; most of the connections are among positive opinionated agents or negative opinionated agents. There exist very few connections between these two groups other than for the agents with extreme opinions. This is expected since the agents with extreme opinions are also those who tend to be more active on social networks for; hence on average, they form more connections. This enables them to be relatively more connected to the agents with opposing opinions. These results are visually depicted in Fig. 2.4 as two snapshots of evolving network diagrams. If $p = 0$, no nudge is applied. In this case, as Fig. 2.4(b) shows, a polarized network, made up of two distinct blue and red-colored clusters, is formed. Blue color corresponds to nodes with $x > 0$, and red color to $x < 0$. The opinion distribution shown in Fig. 2.4(a) confirms the existence of

polarization.

However, when a nudge is applied, even for the case when the nudge probability is as small as $p = 0.01$, we find the network to be well mixed (large blue and red clusters have disappeared) (Fig. 2.4(e)), and this leads to a significantly depolarized state indicated by the approximate unimodality of the opinion distribution as shown in Fig. 2.4(d).

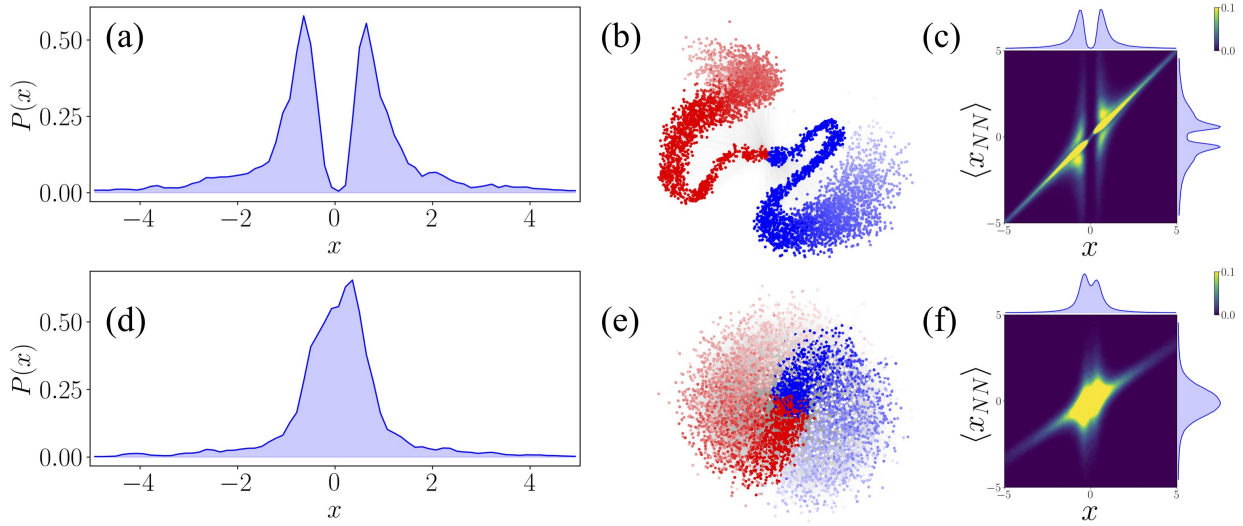


Figure 2.4: Comprehensive analysis showing how random nudges affect opinion distribution, network structure, and echo chamber formation. Top row (a-c): No nudge ($p = 0$) condition showing (a) polarized opinion distribution, (b) segregated network with two distinct clusters (blue nodes for positive opinions, red for negative, with color saturation indicating conviction strength), and (c) two distinct lobes in the heatmap of agent opinions versus their neighbors' mean opinions, confirming strong echo chamber effects. Bottom row (d-f): With nudge ($p = 0.01$) showing (d) depolarized, single-peak opinion distribution, (e) well-mixed network without clear clustering, and (f) single-lobed heatmap confirming the successful weakening of echo chambers. This demonstrates how a small intervention in connection patterns can fundamentally alter the macro-level opinion landscape.

The term echo chamber describes a situation where the beliefs or opinions of people are reinforced by interactions among a closed group of people who hold similar opinions. In recent years, this has been widely discussed in the context of online communities [9–12]. However, some studies appear to suggest that the effects of echo chambers are over-estimated [88]. To infer the presence of echo chamber-type effects, we calculate the average opinion of the nearest neighbors (NN) of each agent [12, 26]. This is denoted by

$$\langle x_{NN} \rangle = k_i^{-1} \sum_j a_{ij} x_j, \quad \text{and} \quad k_i = \sum_j a_{ij}, \quad (2.5)$$

where a_{ij} is the temporally aggregated (over the last 100 time-steps) adjacency matrix. When a nudge is not applied ($p = 0$), a colored heatmap of x and $\langle x_{NN} \rangle$, in Fig. 2.4(c) reveals two disjoint hot spots corresponding to the two distinct echo chambers. And we find a strong bimodality in the marginal distributions. Now, when we apply a nudge with probability $p = 0.01$, we can observe only one hot spot indicating the existence of only one closed group (Fig. 2.4(f)). All the agents are inside this closed group, and the echo chamber effect is largely diluted or non-existent. We did not find perfect unimodality in the marginal distribution of x , which can be attributed to the fact that different realizations can lead to either of these three distributions: (a) slight bimodal distribution with signification reduction in all three polarization parameters, (b) unimodal distribution with a slight skew towards positive opinions and (c) similar distribution with a skew towards negative opinions. As the heat maps and the marginal distributions are created from data averaged over 200 realizations, all the above factors contribute to the slight bimodality in the marginal distribution of x . Nevertheless, the marginal distribution corresponds to a signification reduction in polarization and echo chambers.

2.4.3 Quantitative Analysis of Polarization Reduction

To obtain a global picture of how depolarization sets in as a function of nudge probability p , we plot the three measures of polarization as a function of p . All three measures, $\bar{\Delta}$, Δ_{peak} and σ , have been computed from the simulation results. The results shown represent an average over the last 100 time steps of the simulations and averaged over 200 realizations. In Fig. 2.5, we observe that all three measures of polarization decrease as the strength of the nudge p increases. In particular, $\bar{\Delta}$ and σ are found to decrease as a stretched exponential function $\exp(-p^\gamma)$, and the stretching factor γ is determined through regression to be approximately 0.3. A recent work studying the depolarization of echo chambers [87] considered adding an effective noise term dependent on a random sample of opinions to Eq. (2.2). While this approach succeeds in making the opinion distribution unimodal, it increases the width of the distribution significantly, which as a consequence, corresponds to an increase in extreme opinions. To quantify the effect of the nudge on the extreme opinions, we define f_{ext} as the fraction of agents with conviction $|x| > x_{th}$, where x_{th} is a positive threshold. And indeed our framework of nudging the mechanism of forming social connections in online interactions works well in decreasing width of the opinion distribution (Fig. 2.5 (c)) as well as extreme opinions Fig. 2.5 (d) and also suggests direct algorithmic interventions for recommender systems.

In the original model, the authors found the polarized state to be meta-stable and showed that with an increased value of β , the lifetime of the state has a faster than exponential growth. Our intervention adds more randomness to the system and increases statistical fluctuations. Hence for large p , we observe a drastic decrease in the average lifetime of the polarized and depolarized states. An approximate straight line in the log-log plot indicates the lifetime of polarized or depolarized states decreases as a power law as nudge strength (p) is increased (see Fig. 2.5 (e)). Fig. 2.5 (f) also captures the same effect as we see that radicalization is either non-existent or a rarity for $p < 10^{-2}$, but it increases quickly and becomes a norm for $p > 10^{-2}$.

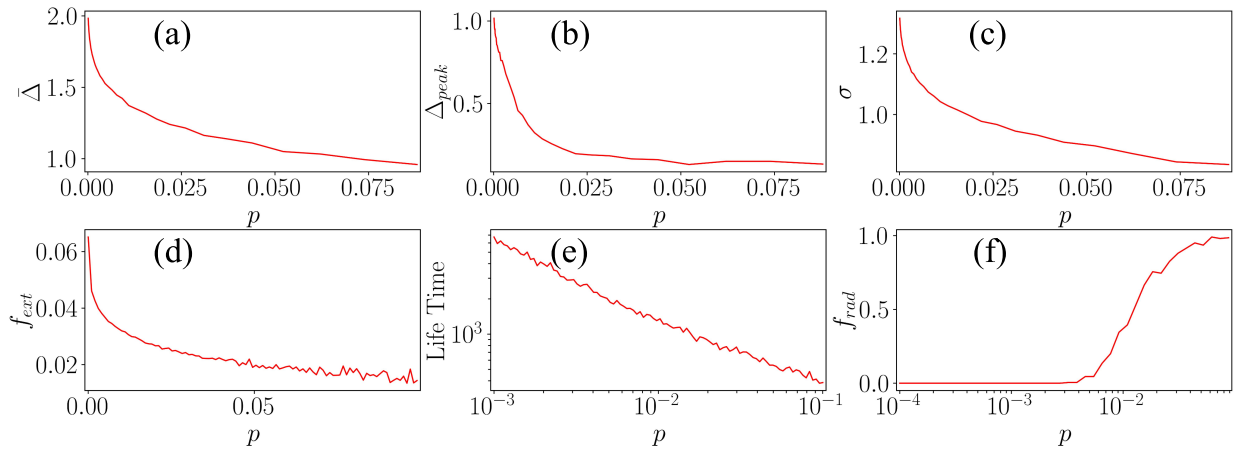


Figure 2.5: Quantitative analysis of polarization measures as functions of nudge strength p . (a-c) Three measures of polarization: (a) $\bar{\Delta}$ (distance between mean opinions), (b) Δ_{peak} (distance between peaks), and (c) σ (standard deviation of opinions) all decrease with increasing nudge strength, following an approximate stretched exponential decay. (d) The fraction of agents with extreme opinions (f_{ext}) similarly decreases, showing the nudge reduces extremism alongside polarization. (e) The lifetime of polarized states decreases as a power law with increasing nudge strength, indicating faster transitions to radicalization state. (f) The fraction of simulations resulting in radicalization increases sharply beyond $p \approx 10^{-2}$, revealing the critical threshold where the intervention begins producing undesirable outcomes. All results represent averages over 200 simulations, excluding radicalized cases for panels (a-d).

2.5 Balancing Depolarization Against Radicalization Risk

In many situations, radicalization is as much undesirable as polarization. Hence to solve the issue of radicalization at a high value of nudge probability, rather than nudging all the people in the population, at each time step of the simulation, we randomly select f fraction of the population and nudged them. We define a simple linear utility function $U(\bar{\Delta}, f_{rad}) = \tilde{\bar{\Delta}} + f_{rad}$ Where $\tilde{\bar{\Delta}}$ is $\bar{\Delta}$, linearly scaled to be between 0 and 1, and f_{rad} is the fraction of radicalized simulations. The

structure of the utility function is the same for the other two measures of polarization.

2.5.1 Finding the Sweet Spot: Optimizing the Nudge

This utility function represents a fundamental trade-off: we want to minimize both polarization (measured by $\bar{\Delta}$) and the risk of radicalization (f_{rad}). In practical terms, this means finding intervention parameters that create enough opinion diversity to prevent echo chambers, but not so much randomness that the system tips into a radicalized state.

Fig. 2.6 depicts the heat map of the utility functions corresponding to the three utility functions. The optimal population fraction and nudge probability is numerically found to follow the curve $p \cdot f^A = B$, where A and B are constants.

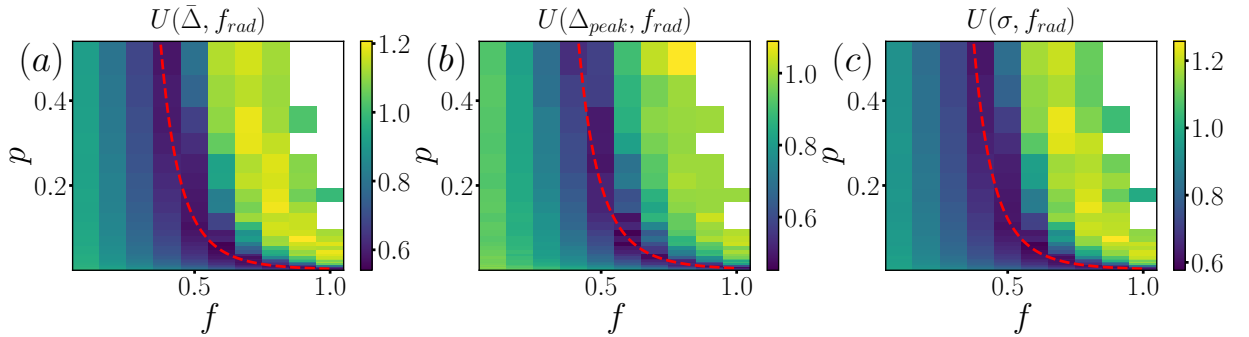


Figure 2.6: Optimization analysis for balancing depolarization against radicalization risk. The heatmaps show utility values (combining polarization reduction and radicalization avoidance) as functions of nudge strength p and population fraction f being nudged. Panels (a), (b), and (c) correspond to utilities based on $\bar{\Delta}$, Δ_{peak} , and σ measures respectively. The red dashed curves, following $p \cdot f^A = B$ (where A and B are constants), indicate the optimal parameter combinations that maximize depolarization while minimizing radicalization risk. This analysis provides practical guidance for implementing nudge strategies in real-world systems by showing that nudging a smaller fraction of the population more strongly can be as effective as nudging everyone weakly.

This power-law relationship reveals an important insight: there's a mathematical trade-off between how many people we nudge (f) and how strongly we nudge them (p). For example, it suggests that nudging 10% of the population with a stronger intervention might be as effective as nudging everyone with a weaker intervention. This finding has significant practical implications for platform design, as it means targeted interventions could potentially be as effective as system-wide changes while requiring less disruption to the overall user experience.

2.6 Robustness Check: Testing on Alternative Models

To ensure the robustness of our intervention framework, we applied network nudge to another recent model [89] of opinion dynamics, which, together with homophily, exhibits the effect of echo chambers. This validation demonstrates that the random nudge strategy is not limited to a single model but represents a more general principle for disrupting echo chambers across different mathematical frameworks. The dynamics of the model is governed by the following N coupled differential equations:

$$\dot{x}_i(t) = |x_i| \sin(x_i^0 - x_i) + K \left(\sum_{j=1}^N A_{ij}(t) \sin(x_i - x_j) \right). \quad (2.6)$$

In contrast to the original model [89], the variable x_i is chosen to be the opinions of the people on a single topic, and the temporal adjacency matrix is formed according to homophily probability (2.3). x_i^0 is the initial opinion of agent i , and all the other variables and parameters have the same meaning as in the previous model (2.2). In Fig. 2.7, we show that When the social interaction and the homophily factor are high enough ($K = 4$, $\beta = 4$), many echo chambers are formed, which is clear from the trajectories of the opinion as well as from the multiple communities seen in the aggregated network (Fig. 2.7 (a, b)). But when we introduce a slight nudge ($p = 0.002$), The effect of echo chambers is reduced drastically. The opinion trajectories seem to converge to a moderate value, and the interaction network is well-connected without any obvious segregated communities (Fig. 2.7 (c, d)).

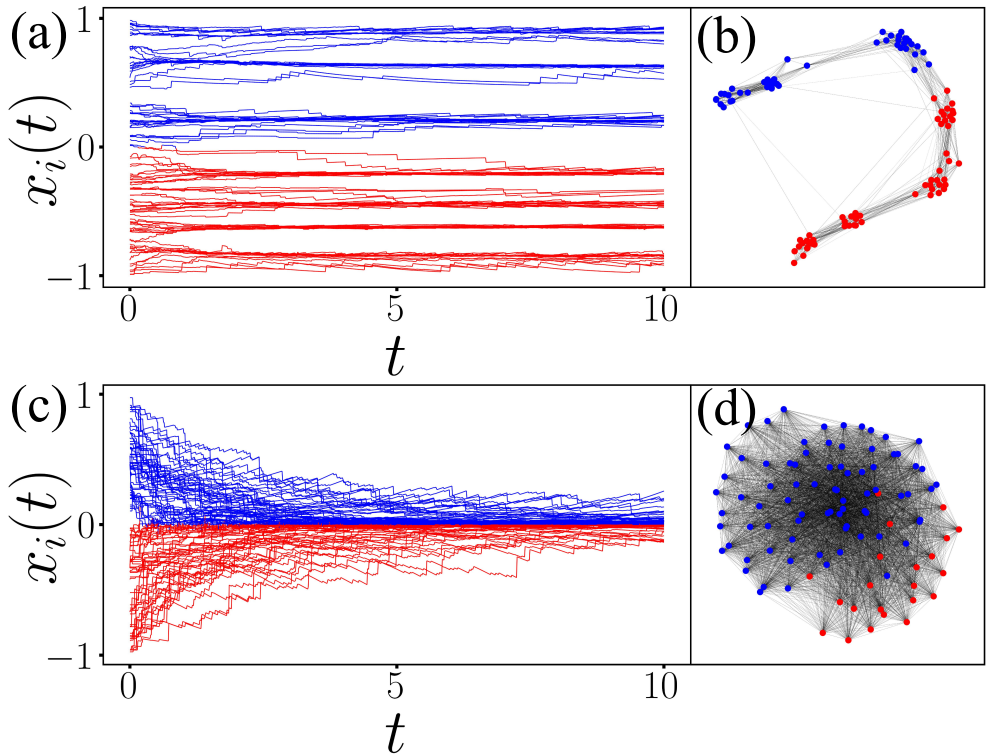


Figure 2.7: Demonstration of the random nudge effectiveness in an alternative opinion dynamics model (Equation (2.6)). **(a)** Without nudge: Opinion trajectories display multiple stable clusters, showing the formation of several distinct echo chambers. **(b)** The corresponding interaction network shows clear community structure with limited cross-group connections. **(c)** With a small nudge ($p = 0.002$): Opinion trajectories converge toward moderate values, showing successful depolarization. **(d)** The resulting interaction network becomes well-connected without distinct communities. This cross-model validation confirms that the random nudge strategy represents a robust intervention principle applicable across different mathematical frameworks of opinion dynamics.

2.7 Discussion and Implications

The widespread use of the internet, and consequently, social media platforms, have drastically altered the way humans consume and interact with information. Polarization and the formation of echo chambers have been shown to negatively impact constructive discussions and debates – two fundamental pillars of a healthy democracy. Building on the recent advances in the modeling of opinion dynamics in social networks, in this work, we study the possibility of depolarizing a population using a stochastic nudge. The implications of our findings extend beyond digital platforms to broader questions about how collective opinions shape societal outcomes and decision-making processes.

2.7.1 Implications for Digital Platform Design

Our results suggest that a small number of randomized interactions, which are other dominated by homophily-driven mechanisms, can lead to a significant reduction in polarization. This reduction was quantitatively captured by three different measures of polarization. While we show that minimal nudges can burst echo chambers and lead to socially desirable distributions of opinions, increasing the strength of this nudge can result in radicalization. Given this sensitivity on the nudge strength, we show that a possible resolution is obtained if, instead of nudging each agent, only a fraction f of the agents are nudged. We highlight that this interplay of the nudge strength p and the fraction f of nudged individuals leads to an interesting optimization problem. This optimization can help inform the fraction of individuals to be nudged for a fixed nudge strength for optimal depolarization.

2.7.2 Ethical Considerations and Implementation Challenges

We believe that the strongest case for the application of such randomized nudges can be made to recommendation systems. While ubiquitous, recommender algorithms are optimized for increasing engagement [90], which we now know can come at the cost of creating echo chambers [91], increase in the representation of extreme ideologies [92], and even the tampering of users' preferences [93]. In such settings, the randomized nudges can be potentially operationalized as the poisoning of a viewer's watch history with a limited amount of random content, uncorrelated with the viewer's preferences [94]. While there are several ethical and legal considerations that must be accounted for before implementing any such interventions, it certainly opens up several interesting avenues for future research to build on. Non-invasive interventions may be important to reduce the detrimental effects of polarization. However, an important first step is to build reliable tools to quantify polarization from data [95], which in itself constitutes an intriguing direction for future research.

2.7.3 Broader Implications for Collective Decision-Making

The random nudge offers a promising, algorithmically implementable strategy for addressing polarization at the individual level. However, this raises important questions about how individual-level interventions might affect collective decision-making processes. The statistical principles underlying opinion formation and the emergence of consensus or polarization may manifest across different scales of human organization. Understanding these connections becomes par-

ticularly relevant when considering how societies make collective choices and how the quality of public discourse influences the outcomes of democratic processes. These insights motivate further investigation into the statistical patterns that govern competitive dynamics in various forms of collective decision-making.

In the next chapter, we will shift our focus from opinion dynamics to electoral systems, examining empirical data from elections across different countries. While not directly employing the opinion models developed here, the underlying theme of how individual choices aggregate into collective outcomes remains central. By analyzing the statistical patterns in election margin distributions, we will uncover universal properties that emerge across diverse electoral systems. These patterns provide a different but complementary perspective on how collective decision-making processes operate at scale, offering insights into the robustness and predictability of democratic institutions regardless of their specific implementation details.

CHAPTER 3

Digging into the Data: The Foundation of Electoral Analysis

In the previous chapter, we explored how random nudges can effectively reduce polarization in online social networks. We now shift our focus to a different but related arena of collective decision-making: democratic elections. Just as individual opinions can aggregate into social patterns, individual votes aggregate into electoral outcomes. Elections represent the ultimate test of democratic opinion dynamics at scale, where millions of citizens express their preferences through a structured process. However, before we can uncover any meaningful patterns or universals in electoral behavior, we must first establish a solid empirical foundation through careful data collection, preparation, and analysis.

3.1 The Pivot: From Opinions to Elections

Individual opinions ultimately aggregate into collective choices through elections. While the previous chapter dealt with the dynamics of opinion formation and the potential interventions to mitigate polarization, this chapter focuses on the empirical foundation of electoral analysis. Elections represent the most structured and widespread manifestation of collective decision-making, offering a rich dataset for studying how individual preferences translate into societal outcomes.

The quality of data is paramount for any meaningful electoral analysis. Without robust, comprehensive, and well-curated data, theoretical insights remain untethered from reality. This chapter details our extensive data collection and preparation efforts, establishing the empirical backbone that will enable the discovery of universal patterns in subsequent chapters.

3.2 Data Collection Methodology and Sources

To conduct a comprehensive analysis of electoral patterns across different democratic systems, we compiled election data from 34 countries spanning six continents. Our data collection began with an ambitious survey of 180 countries and territories worldwide, from which we ultimately selected 34 countries that met our stringent quality criteria for statistical analysis.

Our primary data sources included the Constituency-Level Election Archive (CLEA) website

for constituency-level data of lower chamber legislative elections across the globe [71]. For specialized datasets, we collected polling booth level data for India and Canada directly from their respective Election Commission websites [70, 72], employing semi-automated techniques using Python libraries to handle the diverse data formats. County-level data for the United States was obtained from the MIT Election Data and Science Lab [73].

The data collection process faced considerable technical challenges due to the heterogeneous formats in which electoral data is published worldwide. While constituency-level data from CLEA was consistently formatted in tabular structures, polling booth-level data presented significant extraction challenges, ranging from structured tabular formats to machine-generated and scanned PDFs. We developed robust data cleaning procedures using combinations of Python libraries to handle these varied formats systematically.

For countries like India, we successfully collected data across multiple electoral scales that span three orders of magnitude in voter numbers. At the finest granularity, polling booth level data encompasses approximately 10^2 voters per unit, assembly constituency level data covers approximately 10^5 voters, and parliamentary constituency level extends to approximately 10^6 voters. This multi-scale approach enables investigation of scale-dependent electoral phenomena that have rarely been studied systematically across such a broad range of democratic contexts.

3.3 Dataset Structure and Variable Definitions

The raw election data collected across various countries contained several essential variables that form the foundation of our electoral analysis. Voter turnout represents the actual number of voters who cast ballots in each electoral unit, serving as a crucial scale parameter for our statistical models. Candidate vote tallies provide the detailed breakdown of votes received by each competing candidate, from which we derive winner and runner-up vote counts. The winning margin, defined as the difference between votes secured by the winner and runner-up, captures the competitiveness of each electoral contest. Geographic and administrative identifiers enable spatial analysis and constituency-level comparisons, while temporal information spanning election dates and cycles allows for longitudinal analysis across multiple electoral cycles.

The scale hierarchy in our dataset presents unprecedented opportunities for multi-scale electoral analysis. Indian election data exemplifies this hierarchical structure most comprehensively, encompassing polling booth level data with typical turnouts around 583 voters, assembly constituency level with approximately 116,577 voters for general elections and 86,484 voters for

state elections, and parliamentary constituency level reaching 587,329 voters on average. This three-orders-of-magnitude variation in electoral unit sizes enables systematic investigation of how electoral statistics scale with voter population, a phenomenon that has received limited systematic study in the electoral systems literature.

3.4 Data Processing and Quality Assurance

The raw data required extensive cleaning and standardization procedures to ensure analytical integrity. Our systematic data cleaning approach addressed multiple technical challenges inherent in cross-national electoral data compilation. Missing values were handled through careful exclusion of affected data points rather than imputation, preserving the authenticity of electoral outcomes. Format inconsistencies were systematically standardized, with particular attention to turnout and margin calculations to ensure cross-country comparability. Encoding issues, particularly prevalent in data from countries using non-Latin script languages, were resolved through comprehensive Unicode normalization procedures.

Statistical robustness requirements drove our implementation of stringent filtering criteria that ultimately shaped our final dataset. We established a minimum threshold of 400 consolidated data points per country to ensure adequate statistical power for universality demonstration while maintaining capability for electoral fraud detection. This threshold proved effective for identifying potential electoral misconduct in Ethiopia and Belarus while preserving robust statistical foundations for analysis. Cases with zero turnout were systematically excluded from analysis, as were electoral units with fewer than two competing candidates, ensuring that our margin calculations reflected genuine electoral competition.

Our filtering criteria necessitated significant dataset reduction from the initial survey of 180 countries to the final analytical set of 34 countries. This reduction prioritized data quality over mere quantity, ensuring that each included country contributed statistically meaningful information to our cross-national analysis. To maintain consistency in our turnout calculations, we defined turnout as the sum of valid votes received by all candidates in each electoral unit, avoiding discrepancies that might arise from different approaches to calculating voter participation rates.

The temporal consolidation of multiple elections from each country created unified statistical ensembles that capture long-term electoral patterns while maintaining sufficient sample sizes for robust statistical inference. For Indian elections specifically, our dataset spans from 1962 to 2019 for parliamentary constituencies, 1999 to 2019 for assembly constituencies in general elections,

2004 to 2019 for polling booth level data, and 1961 to 2023 for state assembly elections, providing comprehensive temporal coverage across multiple electoral scales and types.

3.5 Descriptive Statistics and Cross-National Patterns

Our cleaned and standardized dataset reveals remarkable diversity in electoral patterns across countries and scales, providing insights into the fundamental characteristics of democratic competition worldwide. The consolidated electoral data demonstrates substantial variation in mean turnout values, ranging from Denmark's constituency-level average of approximately 2,700 voters to India's parliamentary constituency average exceeding 587,000 voters. Similarly, mean margins of victory exhibit considerable cross-national variation, reflecting different degrees of electoral competitiveness across democratic systems.

The temporal depth of our dataset provides exceptional analytical power, with some countries contributing over 150 years of electoral history. The United States congressional district data spans from 1788 to 2020 across 167 elections, while the United Kingdom's constituency data covers 1832 to 2019 through 46 electoral cycles. This extensive temporal coverage enables investigation of long-term electoral trends and system evolution across different democratic contexts.

Table 3.1 presents comprehensive summary statistics for our dataset, illustrating the extraordinary diversity of electoral scales and patterns across different democratic systems. The table demonstrates the multi-scale nature of our analysis, with electoral unit sizes varying by more than three orders of magnitude within single countries and by over four orders of magnitude across the complete dataset.

The summary statistics reveal several fundamental patterns in our comprehensive dataset. Electoral unit scales demonstrate extraordinary variation both within and across countries, exemplified by the contrast between Canadian polling booths averaging 556 voters and Indian parliamentary constituencies averaging 587,329 voters. The consolidated number of electoral units provides insight into the statistical power available for each country, ranging from Ethiopia's limited 492 units to India's extensive polling booth dataset encompassing 752,786 units.

Cross-national analysis reveals significant differences in electoral competitiveness as measured by the margin-to-turnout ratio. Countries like Denmark and Solomon Islands exhibit relatively high competitiveness with smaller margins relative to turnout, while others show broader victory margins suggesting different competitive dynamics. These variations reflect the complex interplay of electoral systems, political culture, and institutional arrangements across different

democratic contexts.

The temporal coverage demonstrates the robustness of our longitudinal analysis, with consolidated data representing decades or centuries of democratic evolution. Countries like Australia contribute 37 elections from 1901 to 2016, while Canada's constituency-level data spans an remarkable 43 elections from 1867 to 2019. This extensive temporal depth enables investigation of how electoral patterns evolve over time within stable democratic systems, providing insights into the persistence or change of competitive structures across different historical periods.

Table 3.1: Summary Statistics of Election Data

| Country | Time span | Number of elections | Scale | Mean turnout | Mean margin | Number of electoral units (consolidated) |
|---------------------|-----------|---------------------|------------------------|--------------------|--------------------|--|
| Australia | 1901-2016 | 37 | Constituency | 7.37×10^4 | 1.31×10^4 | 1740 |
| Bangladesh | 1973-2008 | 4 | Constituency | 1.57×10^5 | 3.15×10^4 | 1188 |
| Belarus | 2004-2019 | 5 | Constituency | 4.83×10^4 | 2.61×10^4 | 441 |
| Canada | 1867-2019 | 43 | Constituency | 2.76×10^4 | 5.50×10^3 | 10662 |
| Canada | 2004-2021 | 7 | Polling Booth | 5.56×10^2 | 1.35×10^2 | 489919 |
| Chile | 1945-2017 | 7 | Constituency | 1.07×10^5 | 1.05×10^4 | 420 |
| Denmark | 1849-2019 | 30 | Constituency | 2.70×10^3 | 4.64×10^2 | 2178 |
| Ethiopia | 2010-2010 | 1 | Constituency | 4.95×10^4 | 4.18×10^4 | 492 |
| France | 1973-2017 | 3 | Constituency | 7.88×10^4 | 1.10×10^4 | 1712 |
| Germany | 1871-2017 | 19 | Constituency | 1.37×10^5 | 2.26×10^4 | 5108 |
| Ghana | 1992-2016 | 6 | Constituency | 3.75×10^4 | 9.88×10^3 | 1410 |
| Hungary | 1990-2018 | 6 | Constituency | 5.32×10^4 | 8.57×10^3 | 936 |
| India | 1951-2019 | 18 | Constituency | 5.69×10^5 | 8.33×10^4 | 8389 |
| India | 2004-2019 | 4 | Polling Booth | 5.82×10^2 | 1.89×10^2 | 752786 |
| Japan | 1947-2017 | 26 | Constituency | 2.88×10^5 | 2.35×10^4 | 4603 |
| Kenya | 1961-2013 | 2 | Constituency | 3.72×10^4 | 1.19×10^4 | 417 |
| Korea | 1948-2012 | 13 | Constituency | 6.17×10^4 | 1.01×10^4 | 2258 |
| Lithuania | 1992-2020 | 8 | Constituency | 3.24×10^4 | 3.98×10^3 | 570 |
| Malawi | 1994-2019 | 4 | Constituency | 2.31×10^4 | 6.29×10^3 | 755 |
| Malaysia | 1959-2018 | 13 | Constituency | 3.41×10^4 | 8.90×10^3 | 2199 |
| Myanmar | 2010-2015 | 2 | Constituency | 6.76×10^4 | 2.32×10^4 | 634 |
| New Zealand | 1943-2020 | 9 | Constituency | 3.04×10^4 | 6.94×10^3 | 637 |
| Nigeria | 2003-2019 | 2 | Constituency | 7.75×10^4 | 2.20×10^4 | 710 |
| Pakistan | 1988-2013 | 3 | Constituency | 1.28×10^5 | 2.45×10^4 | 683 |
| Papua New Guinea | 1972-2017 | 8 | Constituency | 5.07×10^4 | 5.66×10^3 | 841 |
| Philippines | 1946-2013 | 17 | Constituency | 1.83×10^5 | 2.63×10^4 | 2525 |
| Solomon Islands | 1967-2019 | 14 | Constituency | 3.67×10^3 | 4.37×10^2 | 543 |
| Taiwan | 1986-2020 | 11 | Constituency | 2.33×10^5 | 1.98×10^4 | 482 |
| Tanzania | 2005-2020 | 2 | Constituency | 5.37×10^4 | 2.01×10^4 | 492 |
| Thailand | 1969-2011 | 12 | Constituency | 1.86×10^5 | 1.46×10^4 | 2263 |
| Trinidad and Tobago | 1925-2020 | 13 | Constituency | 1.53×10^4 | 5.12×10^3 | 411 |
| Uganda | 2006-2021 | 4 | Constituency | 4.45×10^4 | 1.08×10^4 | 1430 |
| UK | 1832-2019 | 46 | Constituency | 3.43×10^4 | 6.30×10^3 | 23105 |
| Ukraine | 1998-2019 | 5 | Constituency | 8.89×10^4 | 1.67×10^4 | 1072 |
| United States | 1788-2020 | 167 | Congressional District | 1.14×10^5 | 2.96×10^4 | 33946 |
| United States | 2000-2020 | 6 | County | 1.78×10^5 | 2.00×10^4 | 18905 |
| Zimbabwe | 2005-2018 | 4 | Constituency | 1.77×10^4 | 6.55×10^3 | 743 |

3.6 Dataset Validation and Analytical Framework

This comprehensive dataset represents the empirical foundation upon which our discovery of electoral universality rests. The systematic collection, cleaning, and validation of data from 34 countries across six continents provides unprecedented analytical power for investigating fundamental patterns in democratic competition. Our dataset encompasses over 2.3 million electoral units when consolidated across all countries and scales, representing one of the most extensive cross-national electoral databases assembled for statistical physics analysis.

The quality-first approach in our data curation proves essential for uncovering robust statistical patterns. Rather than pursuing maximum geographical coverage, we prioritized statistical robustness by maintaining stringent quality thresholds for each included country. This methodology enabled us to demonstrate genuine universality in electoral statistics while providing sufficient statistical power to detect deviations indicative of electoral irregularities.

The multi-scale architecture of our dataset, particularly exemplified by the Indian election data spanning three orders of magnitude in electoral unit size, enables investigation of scale-invariant phenomena that would be impossible with single-scale analysis. The successful collection of polling booth level data for India and Canada, representing hundreds of thousands of electoral units, provides the granular resolution necessary for detecting universal statistical signatures across different scales of democratic aggregation.

With this empirically grounded foundation established, we possess the analytical infrastructure necessary to pursue our central research question: do universal statistical patterns emerge in democratic competition that transcend the specific institutional, cultural, and temporal contexts of individual electoral systems? The subsequent chapters will demonstrate how this carefully curated dataset enables the discovery of remarkable universality in electoral margins when properly scaled, revealing fundamental principles governing competitive democratic processes across vastly different contexts.

CHAPTER 4

Universal Clues in the Ballot Box

Building on the empirical foundation established in Chapter 3, we now embark on a focused search for universal patterns in electoral competition. While elections vary dramatically across democracies in their rules, contexts, and scales, we aim to uncover whether fundamental statistical signatures exist that transcend these differences. This chapter presents a systematic analysis of electoral competition metrics, ultimately revealing a remarkable universality that emerges when examining the appropriate normalized measure of electoral margins.

4.1 The Quest for Electoral Universality: From Previous Attempts to New Approaches

In Chapter 3, we laid the groundwork with extensive electoral data from 34 countries across six continents. With this robust empirical foundation in place, we now turn to the central question: Do universal statistical patterns emerge in democratic competition across vastly different electoral systems?

4.1.1 Historical Approaches to Electoral Universality: Prior Research and Limitations

From a statistical physics perspective, elections represent classic complex systems where simple, universal macroscopic patterns might emerge from numerous microscopic interactions. Just as various physical systems composed of different constituent particles can exhibit the same phase transitions or scaling laws, electoral systems with different rules and contexts might share fundamental statistical signatures when properly analyzed.

Previous research has yielded partial insights but no truly robust universal electoral patterns. Various studies have examined vote share distributions and turnout patterns within specific countries [49–51] or across nations with similar electoral protocols [50, 54]. Yet systematic deviations in these distributions have been repeatedly documented [54, 56–59], attributed to variations in electoral district size and other contextual factors.

4.1.2 Exploring Universality in the Electoral Competition

In this chapter, we undertake a systematic search for universal patterns in electoral data. We first focus on two key variables, the margin of victory and voter turnout. While the former captures the essence of democratic competition across different electoral systems, the latter sets the scale of the election. With extensive election data [70–73] from 34 countries (from 6 continents) spanning multiple decades and electorate scales, we analyze distributions of these variables, gradually uncovering a remarkable universal distribution. Finally, we develop a minimal statistical model that explains this universal pattern, offering insights into the fundamental nature of democratic competition.

4.2 The Electoral Process: A Template

A template of a basic electoral process is as follows. At each electoral unit, candidates compete against each other to win the votes of the electorate, who can cast their vote in favor of only one of the candidates. The candidate securing the largest number of polled votes is declared the winner. This represents the core process in many electoral systems. It is the standard first-past-the-post system followed in many countries, e.g., India, the UK, and the USA. In an instant-run-off system (such as in Australia) or two-round run-offs (such as in France), the final run-off round boils down to this template. Typically, national or regional elections following this template consist of many electoral units made up of polling booths, precincts, constituencies, or counties. These units set a size scale in terms of the number of electorates – polling booth represents the smallest scale, while a constituency (subsuming many polling booths) represents the largest scale. For our analysis, an “election” could be either a national, regional, or even a city-level electoral process encompassing N electoral units, and each unit could be a polling booth, county, or constituency.

In any such election, an informative indicator of the degree of competition and the extent of consensus is the margin of victory. A vanishing margin of victory signifies tight competition and a divided electorate, whereas large margins of victory indicate a decisive mandate and overwhelming consensus in favor of one candidate. Let $c_i, i = 1, 2, \dots, N$, denote the number of candidates contesting an election in the i -th electoral unit. The winning and runner-up candidates receive, respectively, $V_{i,w}$ and $V_{i,r}$ votes such that $V_{i,w} > V_{i,r}$. The margin is given by $M_i = V_{i,w} - V_{i,r}$. If $n_i > 0$ is the size of the electorate, *i.e.*, number of registered voters in i -th unit, then $0 \leq M_i \leq n_i$. However, in practice, only a fraction of the electorate participates in voting. In such cases, the number of voters who show up to cast their vote is termed as the turnout T_i , such that $0 \leq T_i \leq n_i$,

and consequently, the margin is further restricted by $0 \leq M_i \leq T_i$.

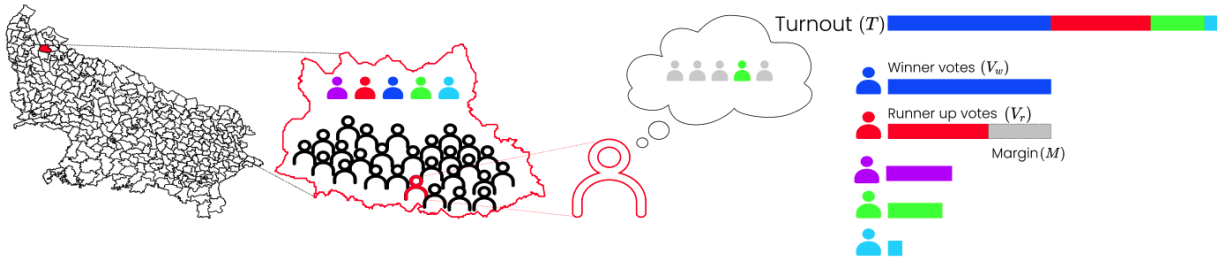


Figure 4.1: Basic template of an election. The map highlights a single electoral unit, within a larger region. In this unit, multiple candidates (colored icons) compete for votes cast by the electorate (black icons). A representative voter casts a ballot for one candidate. The distribution of votes is summarized by key quantities on the right. The *turnout* T (top bar) denotes the number of participating voters and sets the scale of the contest. Among these, the candidate securing the *most votes* (V_w , blue) is declared the winner, while the one with the *second-highest votes* (V_r , red) is the runner-up. The *margin of victory* $M = V_w - V_r$ (gray) quantifies the degree of competition – smaller margins reflect tight races, while larger margins indicate strong consensus. This template abstracts the first-past-the-post electoral mechanism used in countries like India, the UK, and the USA, and serves as the basis for analyzing competitiveness and engagement across electoral units.

4.2.1 The Dance of Turnout and Margin

To fix our ideas, we might focus on the elections in one country, e.g., the general elections in India. Then, the object of interest would be M_i and T_i ($i = 1, 2, \dots, N$). To be statistically robust, the data is consolidated from many elections spread over several decades (For India, 18 elections from 1951 to 2019). This leads to the associated empirical distributions $Q_M(M)$ and $g(T)$, respectively, for margin and turnout. Figure 4.2(a) displays the distribution of raw turnout $g(T)$ at the constituency level for national elections in six countries, namely, India, USA, South Korea, Canada, Japan, and Germany. Striking dissimilarities in $g(T)$ are visible in the shape and support of distribution for countries. For Germany, $g(T)$ has a unimodal character, while that for Canada and the USA display multiple peaks.

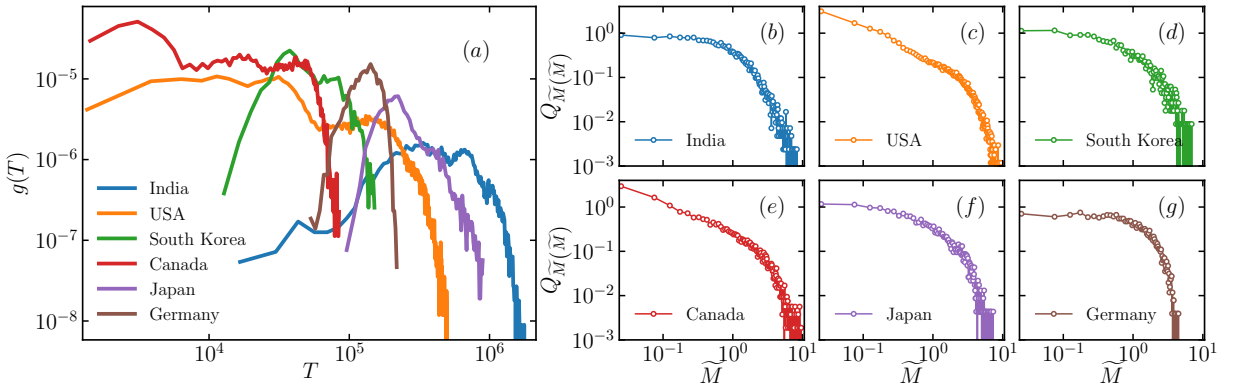


Figure 4.2: (a) Turnout distribution $g(T)$ obtained from election data for different countries. Note the differences in shapes and ranges for $g(T)$. (b-g) Scaled margin distribution $Q_{\widetilde{M}}(\widetilde{M})$ obtained from election data (open circles with solid lines) for India, USA, South Korea, Canada, Japan, and Germany. Despite their distinct electoral systems and political cultures, these distributions show broad similarities but also notable differences in their decay patterns.

Further we scale the margin distribution with the sample mean $\langle M \rangle$, hoping to find a universal pattern. However, as displayed in Fig. 4.2(b-g), the distributions of scaled margin $\widetilde{M} = M/\langle M \rangle$ (computed from the consolidated margin data for each country) demonstrate certain noticeable differences. In particular, $Q_{\widetilde{M}}(\widetilde{M})$ for German elections in Fig. 4.2(g) has a sharp cutoff, but for India and Japan in Fig. 4.2(b, f) the distribution has a slower decay.

Next, we investigate how the electoral scale affects the distributions of our key variables, an essential consideration for any claim of universality. In large countries, depending on the size of the electoral unit, the typical turnout can differ by several orders of magnitude. For example, in India, polling booths have a typical electoral size $\sim 10^3$, whereas, at the parliamentary constituency level, it is about 10^6 . Further, the shapes of $g(T)$ are also vastly different at different scales. Figure 4.3(a) captures the striking differences in range and shape of $g(T)$ for India, the US, and Canada at two different scales. The dashed lines represent smaller scales (polling booths for India and Canada, counties for the USA), while solid lines represent larger scales (constituencies for India and Canada, congressional districts for the USA). The dashed lines represent smaller scales (polling booths for India and Canada, counties for the USA), while solid lines represent larger scales (constituencies for India and Canada, congressional districts for the USA).

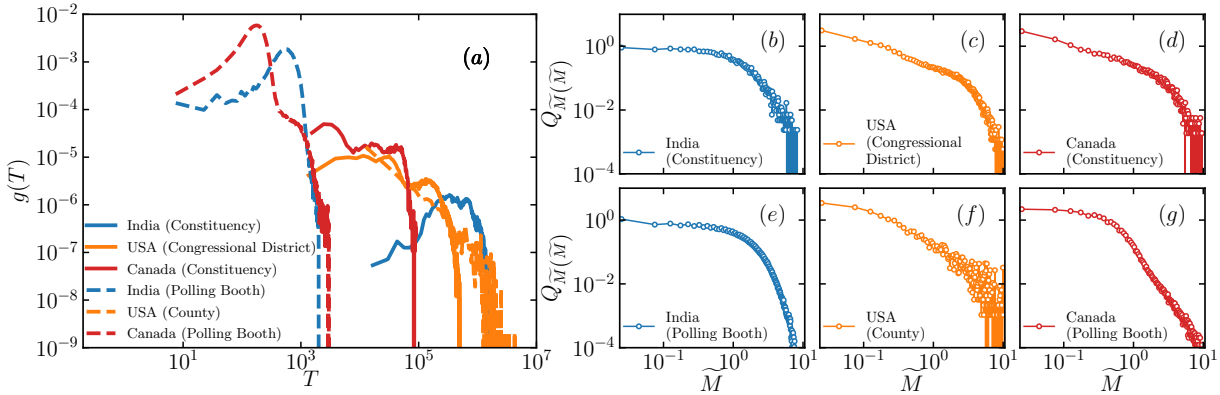


Figure 4.3: The turnout distribution $g(T)$ and scaled margin distribution $Q_{\widetilde{M}}(\widetilde{M})$ for India (blue), the USA (orange), and Canada (red), at two widely different scales, *i.e.*, size of electoral units. (a) $g(T)$ at two different scales for each country. The dashed line is for smaller scales (polling booth for India and Canada, County for the USA), while the solid line represents a larger scale (constituency for India and Canada, congressional district for the USA). (b-g) $Q_{\widetilde{M}}(\widetilde{M})$ from election data (open circles). Despite the differences in scale and shape of $g(T)$, the empirical $Q_{\widetilde{M}}(\widetilde{M})$ shows certain consistent patterns, though scale effects are still evident.

The corresponding scaled margin distributions $Q_{\widetilde{M}}(\widetilde{M})$ are shown in Figure 4.3(b-g). Figure 4.3(b, c, d) shows the empirical distribution of scaled margins (in national elections) at the constituency-level scale, and Figure 4.3(e, f, g) shows the same at the scale of polling booths (county for USA). For each country, the distributions at different scales show certain similarities but also notable differences. For instance, in the USA, the county-level distribution (Figure 4.3(f)) displays a heavier tail compared to the congressional district level (Figure 4.3(c)), reflecting the influence of the underlying turnout distribution. Similar scale-dependent effects are visible in the data from India and Canada.

These variability in the scaled margin distribution, suggests that $Q_{\widetilde{M}}(\widetilde{M})$ still carries the imprint of the underlying turnout distribution and is affected by the scale of electoral units.

4.2.2 The Need for a Scale-Independent Measure

The variations in distributions observed across countries and scales clearly demonstrate that neither raw turnout, nor simple scaled margin can reveal universal patterns in electoral competition. The influence of electoral scale and country-specific factors persists in these measures. This suggests we need a more fundamental approach — one that effectively normalizes out the scale effects while capturing the essential competitive dynamics common to all democratic elections.

Such a measure would need to account for both the margin and the contextual scale of each electoral contest.

4.3 The Specific Margin: A Scale-Invariant Approach

Given the observed dependencies between margins and turnouts, and the constraint that $M \leq T$, we consider a new measure: the specific margin $\mu = M/T$. This ratio represents the margin normalized by the turnout at each electoral unit, producing a measure of electoral competitiveness that is independent of the size of the electorate. The specific margin μ ranges from 0 to 1, where values close to 0 indicate extremely competitive elections (nearly tied results), and values approaching 1 represent complete consensus (where nearly all voters chose the same candidate). By normalizing the margin by the local turnout, we effectively remove the scale dependency that affected our earlier analysis.

4.3.1 Universal Distribution of Scaled Specific Margin

The true breakthrough comes when we examine the scaled specific margin $\tilde{\mu} = \mu/\langle\mu\rangle$, where $\langle\mu\rangle$ is the average specific margin for each country. Figure 4.4 shows the distribution $Q_{\tilde{\mu}}(\tilde{\mu})$ of this scaled specific margin computed from electoral data across 32 countries.

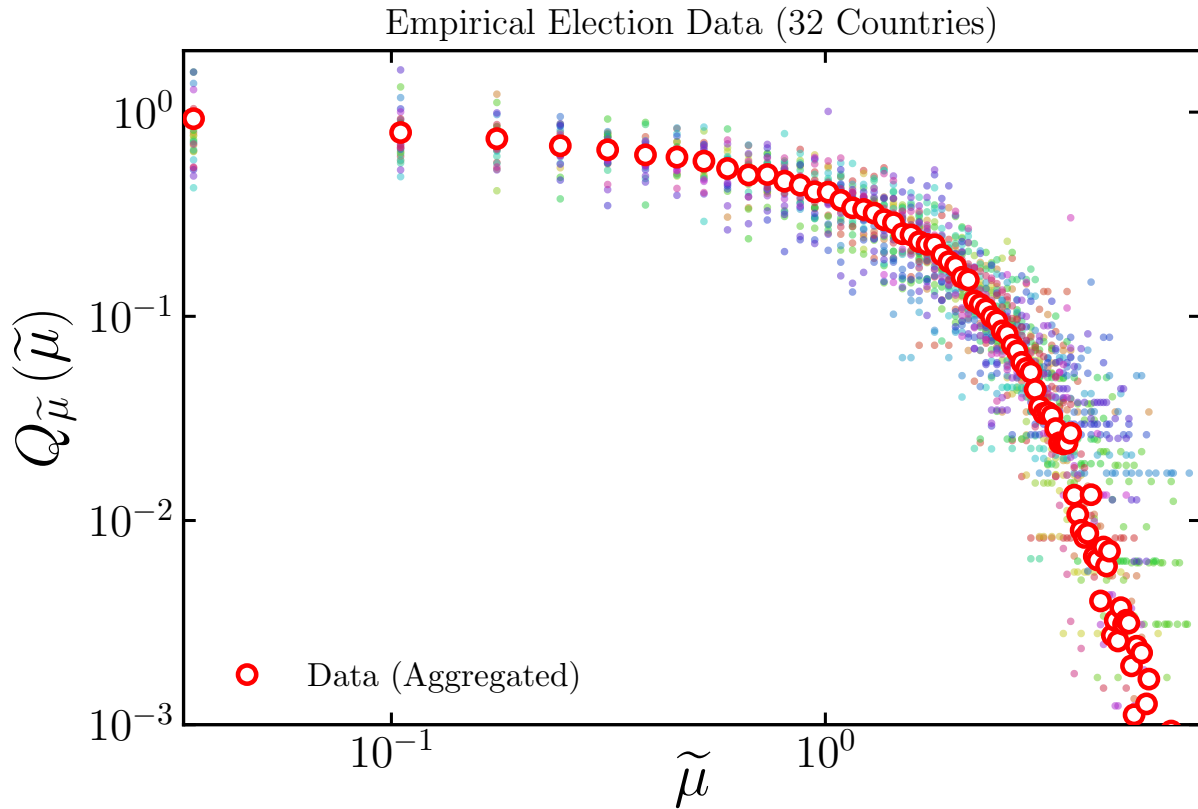


Figure 4.4: The empirical distribution of $\tilde{\mu} = \mu/\langle \mu \rangle$ from election data of 32 countries. Each color indicates a specific country for which the empirical election data is consolidated over several elections. The average of these empirical distributions is shown as red open circles.

Remarkably, Figure 4.4 reveals that the scaled specific margin distributions $Q_{\tilde{\mu}}(\tilde{\mu})$, follows a universal trend across all 32 countries, despite vast differences in their electoral systems, cultural contexts, and historical backgrounds. Each colored point in the figure represents a specific country's data, and while there are small fluctuations around the aggregated distribution (attributable to finite-size effects), the overall pattern is strikingly consistent.

This represents a remarkable finding: despite the immense complexity and diversity of electoral systems worldwide, the scaled specific margin follows a universal distribution, suggesting that the fundamental process of electoral competition—when appropriately normalized—follows the same statistical pattern regardless of where or how the election takes place.

4.4 Theoretical Challenges in Explaining Statistical Universality

While the empirical universality we've discovered is compelling, it raises a fundamental question: Why does this universal pattern emerge across such diverse electoral systems? What underlying mechanism could generate such consistent statistical behavior despite the vast differences in political contexts, voter behaviors, and electoral rules?

4.4.1 A Glimpse of the Mechanism: The Random Voting Model

The consistency of the pattern suggests that there might be a simple but powerful statistical principle at work—something fundamental to the process of competitive selection itself, rather than specific to electoral politics. The universality we've discovered hints that once turnout is “normalized out” through the specific margin, what remains is a fundamental statistical process common to all competitive elections, suggesting that a minimal model focused on the core statistical features of electoral competition might be sufficient to explain the observed universality.

With this insight we propose a simple stochastic model, called the Random Voting Model (RVM). In this model, each voter in a constituency selects one of the candidates according to *some* probability p_j for $j = 1, 2, 3$. While in the next chapter we address the precise choice of these probabilities as well as the detailed analysis of the model, for now, we focus on their statistical consequences. We solve the model in the limit of large turnout ($T \gg 1$), meaning when the number of voters is sufficiently large. In this limit, the votes received by the j -th candidate can be approximated as $v_j \approx p_j T$ (the probability of voting for that candidate multiplied by the turnout), and the margin of victory as $M \approx (p_{(3)} - p_{(2)}) T$, where $p_{(k)}$ denotes the k -th order statistic [96] of the probabilities assigned to the candidates — in simpler terms, $p_{(3)}$ is the probability of the winner and $p_{(2)}$ is the probability of the runner-up. Evidently, in this limit, the specific margin $\mu \approx p_{(3)} - p_{(2)}$ becomes the difference between these probabilities and its distribution has no explicit dependence on turnout T . With this insight, we obtain the distribution of specific margins as:

$$Q_\mu(\mu) = \frac{(1 - \mu)(5 + 7\mu)}{(1 + \mu)^2(1 + 2\mu)^2}. \quad (4.1)$$

Thus, the distribution $Q_{\tilde{\mu}}(\tilde{\mu})$ of the scaled specific margin $\tilde{\mu} = \mu/\langle \mu \rangle$ is:

$$Q_{\tilde{\mu}}(\tilde{\mu}) = \langle \mu \rangle Q_\mu(\tilde{\mu}/\langle \mu \rangle), \quad (4.2)$$

with $\langle \mu \rangle = \frac{1}{2} + \ln \left(\frac{9\sqrt[4]{3}}{16} \right)$ and the distribution is independent of the underlying turnout distribution $g(T)$.

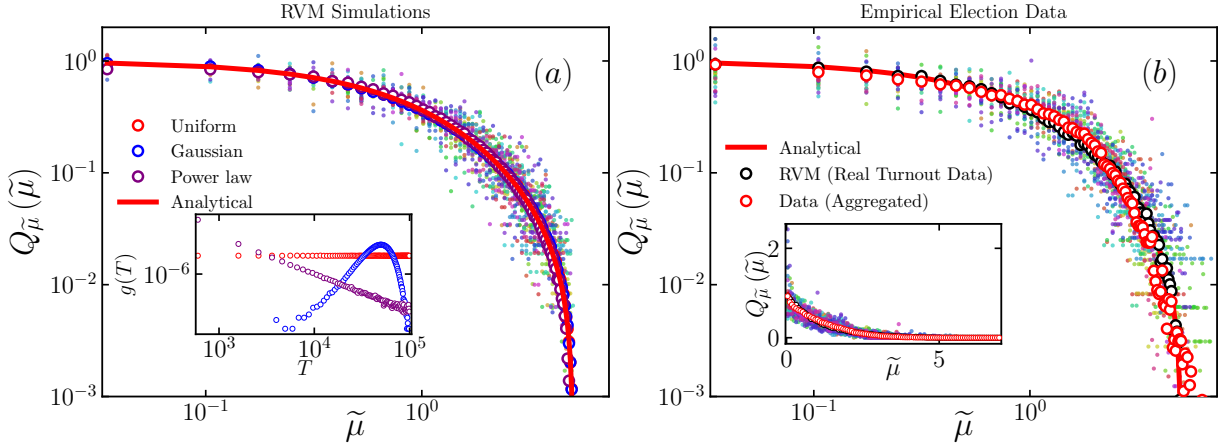


Figure 4.5: (a) $Q_{\tilde{\mu}}(\tilde{\mu})$ predicted by RVM for three different turnout distributions $g(T)$ (see inset). The open circles are obtained from RVM simulations with $N = 10^6$, while the solid colored circles are generated from RVM simulation with N identical to empirical election data. The red line corresponds to $Q_{\tilde{\mu}}(\tilde{\mu})$ in Eq. 4.2. (b) The empirical distribution of $\tilde{\mu} = \mu/\langle \mu \rangle$ from election data of 32 countries (excluding Ethiopia and Belarus). Each color indicates a specific country for which the empirical election data is consolidated over several elections. The average of these empirical distributions (red open circles) closely follows the analytical curve (red line) and the averaged RVM predictions for each country (black open circles). The inset depicts the distributions on a linear scale.

In figure 4.5(a) we demonstrate that $Q_{\tilde{\mu}}(\tilde{\mu})$, computed from RVM simulations with vastly different turnout distributions $g(T)$, does not depend on the detailed structure of $g(T)$ and is in agreement with the analytical prediction in Eq. 4.2. The RVM simulations are performed with 10^6 electoral units using $g(T)$ corresponding to power law, Gaussian, and uniform distributions (inset of Fig. 4.5(a)). The simulated distributions (open circles in Fig. 4.5(a)), for the three cases of $g(T)$, collapse on the analytical prediction $Q_{\tilde{\mu}}(\tilde{\mu})$ (red line).

We further examine if prediction in Eq. 4.2 holds good for the empirical election data. Indeed, as observed in Fig. 4.5(b), the RVM prediction (black open circles) is in excellent agreement with the averaged distributions (open red circles) obtained from all the 32 countries. The averaged empirical distribution is also consistent with the analytical universal curve $Q_{\tilde{\mu}}(\tilde{\mu})$ (red line). Further, the empirical distribution for each of the 32 countries (denoted by the solid-colored circles)

closely follows the trend of $Q_{\tilde{\mu}}(\tilde{\mu})$, albeit with some fluctuations induced by the finite size of data. Similar fluctuations are evident in RVM simulations as well, seen as solid circles in Fig. 4.5(a), when the number of electoral units N is taken from the empirical election data (rather than fixed at 10^6). Empirical distributions shown in the inset of Fig. 4.5(b) demonstrate that at large x , the absolute fluctuations decrease.

Thus, the universality in Fig. 4.5 suggests that irrespective of the finer details of election processes, the mechanism underlying the core component of any competitive election – choosing one candidate from many contenders – leads to a universal distribution for the scaled specific margin $\tilde{\mu} = \mu/\langle\mu\rangle$. This remarkable agreement between our simple Random Voting Model and empirical data from diverse democracies suggests that we have identified a fundamental statistical signature of democratic competition that transcends specific electoral systems and cultural contexts.

4.5 Conclusion: Universality as a Signature of Democratic Competition

In this chapter, using extensive election data from 32 countries spanning multiple decades and electorate scales, we have demonstrated a remarkable statistical universality in democratic electoral competition. While raw turnout distributions vary dramatically across countries and scales, and scaled margin distributions retain country-specific features, the scaled specific margin follows a universal distribution across 32 diverse democracies.

This universality transcends the particularities of individual countries, electoral systems, and scales, revealing what appears to be a fundamental statistical signature intrinsic to competitive democratic processes. Like other universalities discovered in complex systems, this pattern emerges not despite but because of the underlying complexity, as coherent patterns can arise from the aggregation of many individual decisions. We further argue that this universality is a stylized fact of elections and any successful election model should be able to reproduce it.

The elegance of this finding lies in its simplicity: once we properly normalize the margin by the local turnout and scale by the country-specific mean, the resulting distribution follows a consistent pattern regardless of cultural, historical, or institutional factors. It suggests that beneath the surface complexity of electoral politics lies a simpler statistical regularity, which is a signature of democratic competition, which we capture with our proposed Random Voting Model.

Building on the success of the RVM in explaining this universal pattern, the next chapter will provide a comprehensive analysis of the model from first principles. We will derive its mathemat-

ical foundations, demonstrate how it connects turnout distributions to margin distributions across different electoral contexts, and explore how this elegantly simple model can explain multiple empirical findings.

CHAPTER 5

The Random Voting Model: When Chance Explains Choice

In the previous chapter, we uncovered a remarkable universal pattern in electoral statistics: the scaled distribution of the specific margin (margin-to-turnout ratio) follows a consistent curve across diverse democracies, electoral systems, and scales. This universality emerged despite the vast differences in raw turnout and margin distributions across countries. We introduced the Random Voting Model (RVM) as a simple stochastic framework that remarkably captures this universal pattern with surprising accuracy.

Building on this discovery, this chapter provides a comprehensive analysis of the RVM from first principles. We will delve into its mathematical foundations, derive key analytical results, and demonstrate how this elegantly simple stochastic model can explain multiple empirical findings from electoral data. Through both analytical derivations and simulation results, we'll show that the RVM not only predicts the universal specific margin distribution but also connects turnout distributions to margin distributions across different electoral contexts.

5.1 Introducing the Random Voting Model (RVM): Simplicity by Design

The Random Voting Model is based on the premise that electoral outcomes can be understood through a minimal statistical framework that captures the essence of competition without modeling voter psychology or strategic behavior. The model is parameter-free beyond the turnout distribution and number of candidates, relying only on simple probabilistic principles.

In this Random Voting Model, c_i number of candidates contest at i -th electoral unit with n_i electors (voters) and each elector from the i -th electoral unit casts their vote for j -th candidate with a probability p_{ij} . These probabilities are assigned as follows: for each candidate, a number between 0 and 1 is drawn uniformly at random, which is assigned as an unnormalized probability weight w_{ij} to that candidate. The weights are subsequently normalized to get the probability

$p_{ij}, j = 1, 2 \dots c_i$ of receiving the vote of an elector. This can be mathematically stated as

$$w_{ij} \sim \mathcal{U}(0, 1) \quad \text{and} \quad p_{ij} = \frac{w_{ij}}{\sum_k w_{ik}}, \text{ with } j = 1, 2 \dots c_i, \quad (5.1)$$

where $\mathcal{U}(0, 1)$ denotes a uniformly distributed random variable in $(0, 1)$.

After each of the n_i electors (voters) in i -th electoral unit casts their vote for some candidate j independently with probability p_{ij} , the candidate receiving the most votes $V_{i,w}$ is declared the winner, and the candidate securing the next largest number of votes $V_{i,r}$ is the runner-up. The *margin of victory* M_i is then defined to be the vote difference between the winner and the runner-up: *i.e.* $M_i = V_{i,w} - V_{i,r}$. The empirical election data we employ shows that the top three candidates, on average, account for nearly 87% of all votes polled in an election. Hence, as part of the model specification, we fix the number of candidates in each electoral unit to be three, *i.e.*, $c_i = 3$ for all i .

The only input to this model is the raw turnout data, *i.e.*, the number of voters (who actually voted) in each constituency. For the model simulation, we use the turnout data of real elections as the total number of voters in different constituencies. To understand how simulations are performed, consider this notional example: if a country has $N = 100$ constituencies and data for five such elections is available. Then, the model is simulated on 500 electoral units. The number of electors in each electoral unit is taken from the consolidated turnouts. Such a simulation of election is performed multiple times to get the average distributions.

5.2 Analytical Derivation of the Universal Specific Margin Distribution

We now demonstrate how the RVM explains the universal distribution of scaled specific margin $Q_{\tilde{\mu}}$ ($\tilde{\mu}$) observed in the previous chapter. As mentioned in the previous section (5.1), we consider the case where 3 candidates are contesting in an election. The weight assigned for the j -th candidate of the i -th electoral unit is w_{ij} . These weights are drawn independently at random from a uniform distribution between 0 and 1. The corresponding probability p_{ij} of receiving votes is calculated by normalizing these weights. Hence, we have the following,

$$w_{ij} \sim \mathcal{U}(0, 1) \text{ and } p_{ij} = \frac{w_{ij}}{\sum_{k=1}^3 w_{ik}}; \text{ with } j = 1, 2, 3. \quad (5.2)$$

For the rest of the analysis in this chapter, we focus on a single (i -th) electoral unit with voter turnout T and drop the corresponding index i for brevity. Hence,

$$w_{ij} := w_j \text{ and } p_{ij} := p_j. \quad (5.3)$$

5.2.1 The Set-up: Large Turnout Limit

For large turnout ($T \gg 1$), it is reasonable to assume the number of votes received by j -th candidate is proportional to their probability p_j , in particular, $v_j \approx p_j T$. Hence, for $T \gg 1$, the *margin* can be approximated as

$$M \approx (p_{\max} - p_{2nd \max})T, \quad (5.4)$$

where p_{\max} and $p_{2nd \max}$ correspond to the largest and the second largest probabilities assigned to the candidates. For example, if the probabilities p_1, p_2 , and p_3 assigned to the 3 candidates are 0.1, 0.6, and 0.3, then $p_{\max} = p_2 = 0.6$ and $p_{2nd \max} = p_3 = 0.3$. The margin M can also be written in terms of w_j as the following:

$$\begin{aligned} M &\approx \left(\frac{w_{\max}}{w_1 + w_2 + w_3} - \frac{w_{2nd \max}}{w_1 + w_2 + w_3} \right) T, \\ &= \left(\frac{w_{(3)}}{w_{(1)} + w_{(2)} + w_{(3)}} - \frac{w_{(2)}}{w_{(1)} + w_{(2)} + w_{(3)}} \right) T, \\ &= \left(\frac{w_{(3)} - w_{(2)}}{w_{(1)} + w_{(2)} + w_{(3)}} \right) T, \end{aligned} \quad (5.5)$$

where $w_{(k)}$ is the k -th order statistics [96]. Hence,

$$\frac{M}{T} \approx \frac{w_{(3)} - w_{(2)}}{w_{(1)} + w_{(2)} + w_{(3)}}. \quad (5.6)$$

5.2.2 Order Statistics: The Key to Understand Ranking

Consider n *iid* random variables $\{X_1, X_2 \dots X_n\}$ drawn from a distribution $\rho(x)$. When arranged in ascending order, the random variable at the k -th spot is defined as the k -th order statistics. In particular, n -th and 1-st order statistics correspond to the maximum and minimum of those n random variables, respectively. The k -th order statistics of the random variable X is denoted by $X_{(k)}$.

The joint probability density of all the order statistics of the above-mentioned n random variables, $\mathbb{P}(x_{(1)}, x_{(2)}, \dots, x_{(n)})$, defined as the probability density that the random variable $X_{(k)}$ takes the value $x_{(k)}$ for $k \in \{1, 2, \dots, n\}$, is

$$\mathbb{P}(x_{(1)}, x_{(2)}, \dots, x_{(n)}) = n! \prod_{k=1}^n \rho(x_{(k)}). \quad (5.7)$$

5.2.3 Application to the Random Voting Model

Now that we understand the joint probability density of the order statistics, for RVM, we have $n = 3$ and $\rho(x) = \mathcal{U}(0, 1)$. Hence we have,

$$\mathbb{P}(w_{(1)}, w_{(2)}, w_{(3)}) = 3! = 6; \text{ with } 0 < w_{(1)} < w_{(2)} < w_{(3)} < 1, \quad (5.8)$$

and $\mathbb{P}(w_{(1)}, w_{(2)}, w_{(3)}) = 0$ otherwise, with the following normalization:

$$\int_0^1 dw_{(3)} \int_0^{w_{(3)}} dw_{(2)} \int_0^{w_{(2)}} 6dw_{(1)} = 1. \quad (5.9)$$

From the joint probability distribution of all the order statistics, we calculate the approximate probability density function of specific margin $M/T = \mu$ from Eq. (5.6) as follows,

$$\begin{aligned} Q_\mu(\mu) &= 6 \int_0^1 dw_{(3)} \int_0^{w_{(3)}} dw_{(2)} \int_0^{w_{(2)}} \delta\left(\mu - \frac{w_{(3)} - w_{(2)}}{w_{(1)} + w_{(2)} + w_{(3)}}\right) dw_{(1)}, \\ &= 6 \int_0^1 dw_{(3)} \int_0^{w_{(3)}} \frac{w_{(3)} - w_{(2)}}{\mu^2} \mathbb{1}_{0 < \frac{w_{(3)} - \mu w_{(3)} - (1+\mu)w_{(2)}}{\mu} < w_{(2)}} dw_{(2)}, \\ &= 6 \int_0^1 dw_{(3)} \frac{(1-\mu)(5+7\mu)w_{(3)}^2}{2(1+\mu)^2(1+2\mu)^2}. \end{aligned} \quad (5.10)$$

$$(5.11)$$

Finally, after performing this integral, we get

$$Q_\mu(\mu) = \frac{(1-\mu)(5+7\mu)}{(1+\mu)^2(1+2\mu)^2}. \quad (5.12)$$

The distribution $Q_\mu(\mu)$ does not depend on the turnout and is universal. Now, by a change of variable to scaled specific margin defined as $\tilde{\mu} = \mu/\langle\mu\rangle$, we obtain its distribution $Q_{\tilde{\mu}}(\tilde{\mu})$ to be

$$Q_{\tilde{\mu}}(\tilde{\mu}) = \langle\mu\rangle Q_\mu(\tilde{\mu}\langle\mu\rangle) = \frac{\langle\mu\rangle(1 - \tilde{\mu}\langle\mu\rangle)(5 + 7\tilde{\mu}\langle\mu\rangle)}{(1 + \tilde{\mu}\langle\mu\rangle)^2(1 + 2\tilde{\mu}\langle\mu\rangle)^2}, \quad (5.13)$$

where $\langle\mu\rangle = \frac{1}{2} + \ln\left(\frac{9\sqrt[4]{3}}{16}\right)$. This derived distribution $Q_{\tilde{\mu}}(\tilde{\mu})$ is precisely the universal curve observed in the empirical data across 32 countries in the previous chapter. The remarkable agreement between theory and data as shown in Fig. 5.1 confirms that the RVM captures the essential statistical features underlying electoral competition.

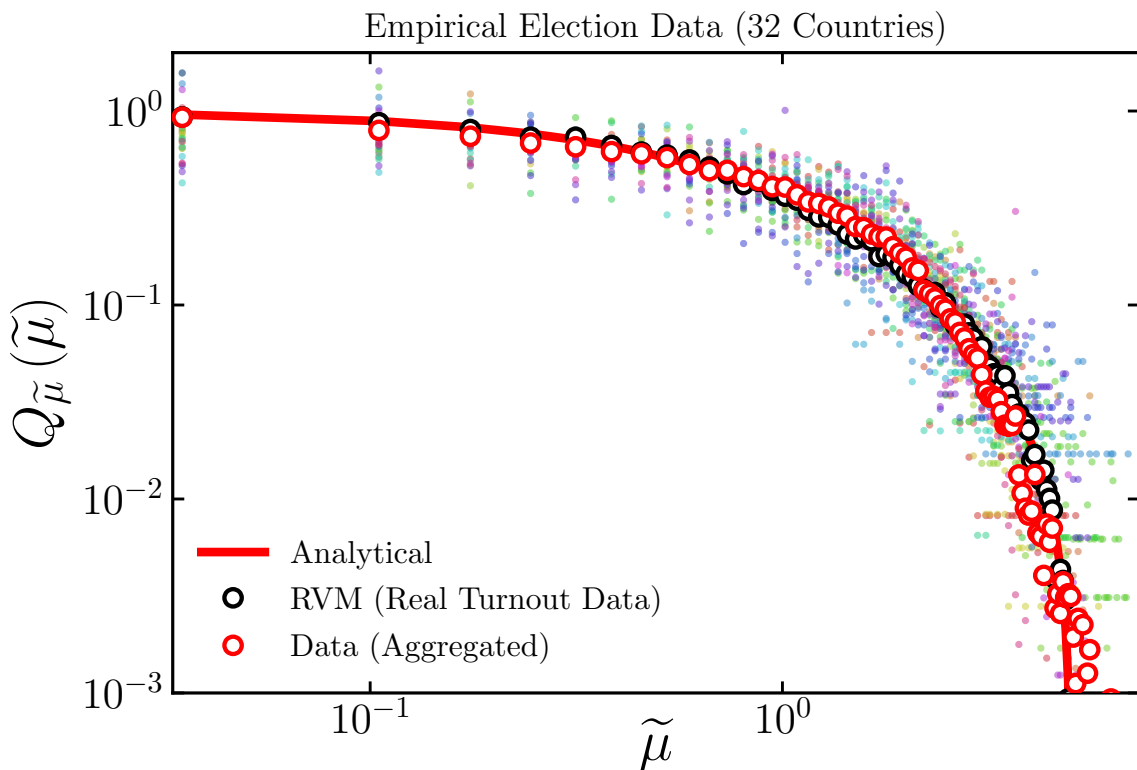


Figure 5.1: $Q_{\tilde{\mu}}(\tilde{\mu})$: The distribution is universal and does not depend on the turnout distribution. Each color indicates empirical $Q_{\tilde{\mu}}(\tilde{\mu})$ for a specific country for which the election data is consolidated over several elections. The average of these empirical distributions (red open circles) closely follows the analytical curve (red line) and the averaged RVM predictions for each country (black open circles).

5.3 Predicting Margin Distributions from Turnout Distributions

Having established that the RVM predicts the universal specific margin distribution, we now explore how the model can predict the margin distribution $Q_M(M)$ from an arbitrary turnout distribution $g(T)$. From the previous section, we have the distribution of the specific margin $\mu = M/T$ to be

$$Q_\mu(\mu) = \frac{(1-\mu)(5+7\mu)}{(1+\mu)^2(1+2\mu)^2}. \quad (5.14)$$

Through a simple change of variable ($M = \mu T$) we get,

$$\mathcal{P}(M|T) = \frac{(1-M/T)(5+7M/T)}{T(1+M/T)^2(1+2M/T)^2}. \quad (5.15)$$

For an arbitrary turnout distribution $g(T)$, we obtain the distribution of M to be,

$$Q_M(M) = \int_M^\infty g(T)\mathcal{P}(M|T)dT = \int_M^\infty g(T) \frac{(1-M/T)(5+7M/T)}{T(1+M/T)^2(1+2M/T)^2}dT. \quad (5.16)$$

Again with $u = T/M$, the above integral transforms to,

$$Q_M(M) = \int_1^\infty g(Mu) \frac{u(u-1)(5u+7)}{(1+u)^2(2+u)^2}du. \quad (5.17)$$

5.3.1 Turnout Distribution Effects on Margin Distribution

We compute $Q_M(M)$ for different turnout distributions $g(T)$. In particular, we take $g(T)$ to be (A) exponential, (B) power law, and (C) Gaussian distributions as they have vastly different tail behaviors. Finally we also consider a uniform turnout distribution with finite support.

5.3.1.1 Exponential Turnout Distribution

In this case $g(T) = \frac{1}{\tau}e^{-T/\tau}$, with $\tau > 0$. Hence,

$$Q_M(M) = \int_1^\infty \frac{1}{\tau}e^{-Mu/\tau} \frac{u(u-1)(5u+7)}{(1+u)^2(2+u)^2}du, \quad (5.18)$$

or,

$$Q_M(M) = \frac{e^{-\frac{M}{\tau}}}{\tau^2} \left(4e^{\frac{2M}{\tau}}(\tau+M)\text{Ei}\left(-\frac{2M}{\tau}\right) - 9e^{\frac{3M}{\tau}}(\tau+2M)\text{Ei}\left(-\frac{3M}{\tau}\right) - 4\tau \right), \quad (5.19)$$

where $\text{Ei}(x) = \int_{-\infty}^x \frac{e^t}{t} dt$. At large margin limit ($M \rightarrow \infty$), the asymptotic behavior of the distribution is the following (up to the leading order of M):

$$Q_M(M) = \frac{\tau}{3M^2} e^{-M/\tau}. \quad (5.20)$$

This suggests that in the large margin limit, both the margin and its corresponding turnout distribution have an exponential decay with the same rate.

5.3.1.2 Power law Turnout Distribution

In this case $g(T) = \frac{\alpha-1}{T_{min}^{1-\alpha}} T^{-\alpha}$, with $\alpha > 1$ and $T > T_{min}$. Hence we have,

$$Q_M(M) = \int_1^\infty \frac{\alpha-1}{T_{min}^{1-\alpha}} (Mu)^{-\alpha} \frac{u(u-1)(5u+7)}{(1+u)^2(2+u)^2} du, \quad (5.21)$$

or,

$$Q_M(M) = C(M) \frac{\alpha-1}{T_{min}^{1-\alpha}} (M)^{-\alpha}, \quad (5.22)$$

where,

$$C(M) = \begin{cases} I_1(\infty) - I_1(T_{min}/M), & \text{if } M \leq T_{min} \\ I_1(\infty) - I_1(1), & \text{otherwise,} \end{cases} \quad (5.23)$$

with,

$$I_1(y) = \int \frac{y^{1-\alpha}(y-1)(5y+7)}{(1+y)^2(2+y)^2} dy, \quad (5.25)$$

and,

$$I_1(y) = \begin{cases} -\frac{4}{y+1} + \frac{9}{2(y+2)} - \frac{1}{4}7\ln(y) + 4\ln(y+1) - \frac{9}{4}\ln(y+2), & \text{if } \alpha = 2 \\ \frac{y^{2-\alpha} \left(16 {}_2F_1(2, 2-\alpha; 3-\alpha; -y) - 9 {}_2F_1(2, 2-\alpha; 3-\alpha; -\frac{y}{2}) \right)}{4(\alpha-2)}, & \text{otherwise,} \end{cases} \quad (5.26)$$

$$I_1(y) = \begin{cases} -\frac{4}{y+1} + \frac{9}{2(y+2)} - \frac{1}{4}7\ln(y) + 4\ln(y+1) - \frac{9}{4}\ln(y+2), & \text{if } \alpha = 2 \\ \frac{y^{2-\alpha} \left(16 {}_2F_1(2, 2-\alpha; 3-\alpha; -y) - 9 {}_2F_1(2, 2-\alpha; 3-\alpha; -\frac{y}{2}) \right)}{4(\alpha-2)}, & \text{otherwise,} \end{cases} \quad (5.27)$$

where ${}_2F_1(a, b; c; z)$ is a hypergeometric function [97], defined as,

$${}_2F_1(a, b; c; z) = \sum_{n=0}^{\infty} \frac{(a)_n(b)_n}{(c)_n} \frac{z^n}{n!} = 1 + \frac{ab}{c} \frac{z}{1!} + \frac{a(a+1)b(b+1)}{c(c+1)} \frac{z^2}{2!} + \dots$$

It is evident from Eq. (5.22) that for $M > T_{min}$, the margin distribution decays with a power law exponent α , exactly the same as the turnout distribution.

5.3.1.3 Gaussian Turnout Distribution

In this case $g(T) = C_0 e^{-(T/T_0)^2}$, with $T > 0$. Hence,

$$Q_M(M) = \int_1^\infty C_0 e^{-(Mu/T_0)^2} \frac{u(u-1)(5u+7)}{(1+u)^2(2+u)^2} du. \quad (5.29)$$

At large margin limit ($M \rightarrow \infty$), the asymptotic behavior of the distribution is the following (up to the leading order of M):

$$Q_M(M) = \frac{C_0}{12} \left(\frac{T_0}{M} \right)^4 e^{-(M/T_0)^2}, \quad (5.30)$$

and it has a Gaussian decay similar to the corresponding turnout distribution.

From the asymptotic analysis of the margin distributions for the three above-mentioned turnout distributions, we provide strong evidence that the tails of the margin distributions mimic that of the corresponding turnout distribution. For completeness, we also compute the margin distribution corresponding to a uniform turnout distribution which has a finite support (no tail behavior).

5.3.1.4 Uniform Turnout Distribution

In this case $g(T) = \frac{1}{b-a}$, when $T \in [a, b]$, otherwise $g(T) = 0$. Hence,

$$Q_M(M) = \begin{cases} \frac{1}{b-a} \int_{a/M}^{b/M} \frac{u(u-1)(5u+7)}{(1+u)^2(2+u)^2} du, & \text{if } M \leq a \\ \frac{1}{b-a} \int_1^{b/M} \frac{u(u-1)(5u+7)}{(1+u)^2(2+u)^2} du, & \text{otherwise,} \end{cases} \quad (5.31)$$

$$Q_M(M) = \begin{cases} \frac{1}{b-a} (I_2(b/M) - I_2(a/M)), & \text{if } M \leq a \\ \frac{1}{b-a} (I_2(b/M) - I_2(1)), & \text{if } a > M \geq b \\ 0, & \text{otherwise,} \end{cases} \quad (5.32)$$

or,

$$Q_M(M) = \begin{cases} \frac{1}{b-a} (I_2(b/M) - I_2(a/M)), & \text{if } M \leq a \\ \frac{1}{b-a} (I_2(b/M) - I_2(1)), & \text{if } a > M \geq b \\ 0, & \text{otherwise,} \end{cases} \quad (5.33)$$

$$Q_M(M) = \begin{cases} \frac{1}{b-a} (I_2(b/M) - I_2(a/M)), & \text{if } M \leq a \\ \frac{1}{b-a} (I_2(b/M) - I_2(1)), & \text{if } a > M \geq b \\ 0, & \text{otherwise,} \end{cases} \quad (5.34)$$

$$(5.35)$$

where,

$$I_2(y) = \int \frac{y(y-1)(5y+7)}{(1+y)^2(2+y)^2} dy = -\frac{4}{y+1} + \frac{18}{y+2} - 4 \ln(y+1) + 9 \ln(y+2). \quad (5.36)$$

5.3.2 RVM Simulations with Synthetic Turnout Distributions

We perform simulation using the following four different synthetic turnout distributions, to further validate our analytical results, specifically the tail behavior of the margin distribution.

1. **Gaussian Turnout Distribution:** $g(T) = \frac{1}{\sigma\sqrt{2\pi}} \exp\left(-\frac{(T-\mu)^2}{2\sigma^2}\right)$, with $\mu = 50000$, $\sigma = 10000$ and $T > 0$.
2. **Exponential Turnout Distribution:** $g(T) = \frac{1}{\tau} \exp\left(-\frac{T}{\tau}\right)$, with $\tau = 50000$.
3. **Power law Turnout Distribution:** $g(T) = \frac{\alpha-1}{T_{min}^{1-\alpha}} T^{-\alpha}$, with $\alpha = 2$ and $T_{min} = 100$ (minimum possible turnout).
4. **Uniform Turnout Distribution:** $T \sim \mathcal{U}(a, b)$, with $a = 100$ and $b = 100000$. $\mathcal{U}(a, b)$ denotes uniform distribution between the range a and b .

Each of the RVM simulations was performed on 10^6 electoral units, with turnouts (rounded down to the nearest integer) drawn from one of these four distributions. The simulation demonstrates that the tail of the margin distribution mimics the turnout distribution's tail. This is evident in Fig. 5.2(a), (b), and (c). The tail of the margin distribution (Fig. 5.2 (c)) corresponding to power law turnouts decays with the same power law exponent. In the simulation with Gaussian turnout distribution, we find the tail of the margin distribution also has a Gaussian falloff (Fig. 5.2 (a)). Similarly, the margin distribution corresponding to exponential turnouts has an exponential tail (Fig. 5.2 (b)). As the probability density function of uniform turnout distribution and corresponding margin distribution have finite supports, their tails can not be properly defined. We find a sharp cutoff in the corresponding margin distribution. The analytical (semi-analytical for Gaussian turnout) predictions for the margin distributions (shown as black lines in Fig. 5.2) corresponding to all four aforementioned turnout distributions are in excellent agreement with the RVM simulation. In empirical county-level election data of the United States, the heavy-tailed decay of the turnout distribution is reflected in the corresponding margin distribution (Fig. 5.2(e)). In Fig. 5.2(f), we see a similar decay trend in both margin and turnout distribution, which correspond to congressional district-level election data of the USA.

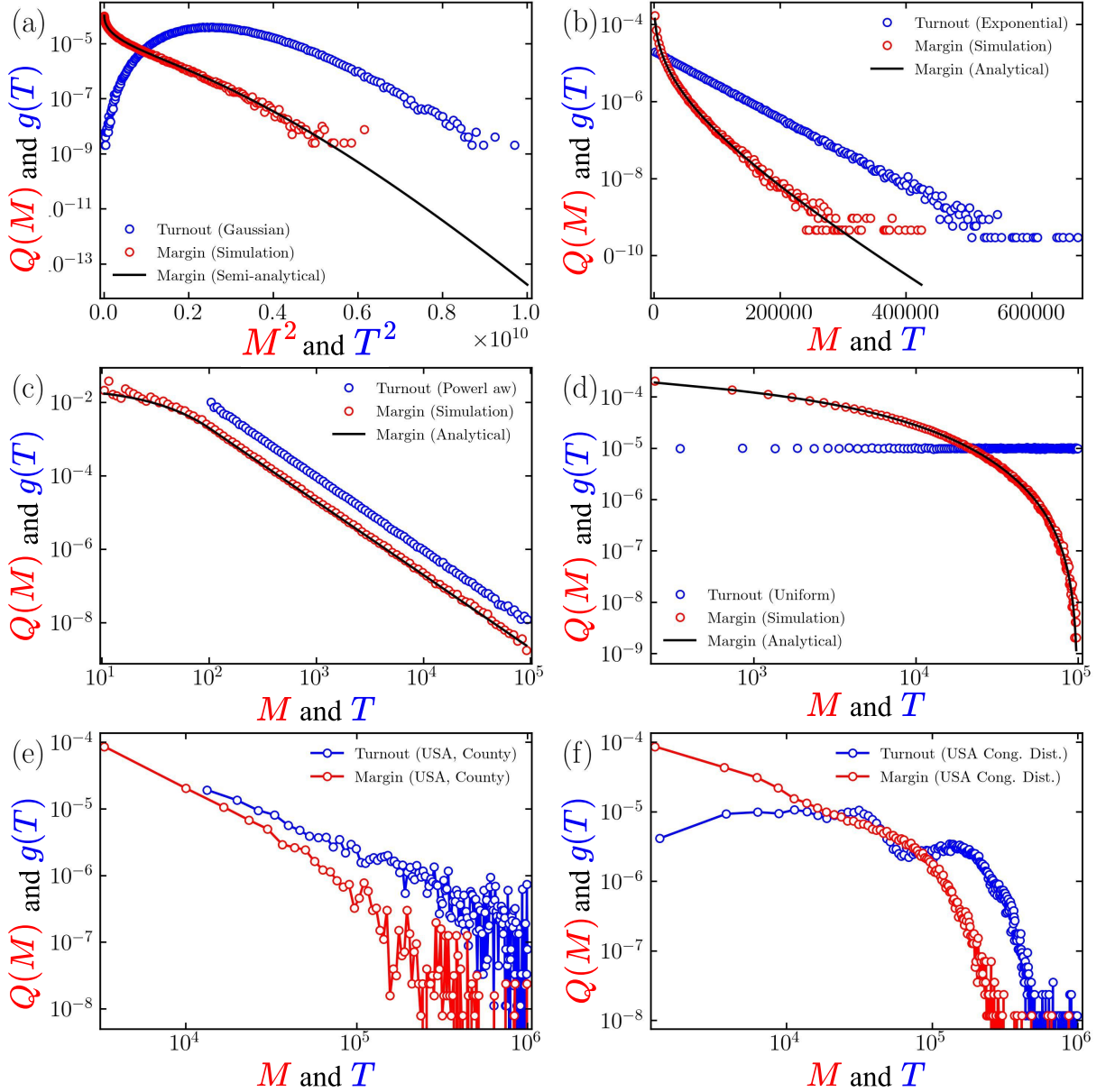


Figure 5.2: The margin distribution $Q_M(M)$ is plotted with the corresponding turnout distribution $g(T)$ to demonstrate that the tails of both these distributions are correlated. Panels (a), (b), (c), and (d) correspond to Gaussian, exponential, power law, and uniform turnout distributions, respectively. Blue open circles denote the turnout distributions. Red open circles denote the margin distribution computed through RVM simulations. Black solid lines correspond to the margin distribution computed using Eq. 5.17. For exponential, power law, and uniform turnout distributions, the integration was analytically calculated, and for Gaussian turnout distribution, it was evaluated numerically. Panels (e) and (f) depict the margin and turnout distribution for the county-level and congressional district-level election data of the USA, respectively.

5.3.3 The Necessity of Scaling in Margin Distribution Analysis

While the RVM successfully explains the shape of the margin distributions $Q_M(M)$ and capture their tail behaviors remarkably well, it fails to predict the empirical mean of those distributions. To overcome this limitation, we scale the margin distribution by its mean $\langle M \rangle$, and investigate the predictive power of the RVM on the scaled margin distribution $Q_{\widetilde{M}}(\widetilde{M})$.

5.3.3.1 Predicting Scaled Margin Distributions Across Countries

As demonstrated in the previous chapter, different countries exhibit vastly different turnout distributions $g(T)$ that reflect distinct electoral systems and contexts. The key question is whether the RVM can capture the resulting variations in scaled margin distributions $Q_{\widetilde{M}}(\widetilde{M})$.

Figure 5.3 (b-g) shows that the RVM predictions (solid lines) achieve excellent agreement with empirical scaled margin distributions (open circles) across diverse countries including India, USA, South Korea, Canada, Japan, and Germany. Notably, the model faithfully captures the disparate decay features observed in different countries — from the sharp cutoff characteristic of German elections to the heavier tails seen in Indian and Japanese data. This demonstrates that raw turnout data carries intrinsic information about the margin distribution, which the RVM effectively leverages without requiring any parameter tuning.

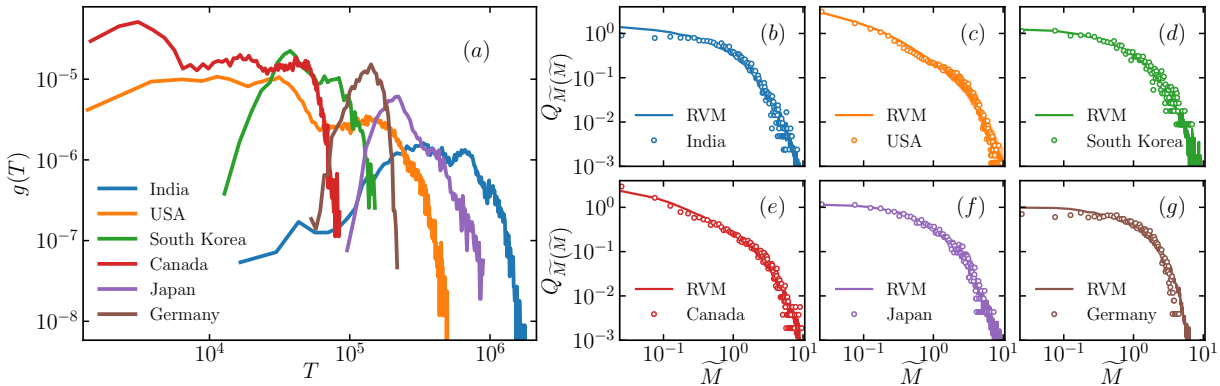


Figure 5.3: RVM predictions of scaled margin distributions across diverse electoral systems. (a) Turnout distributions $g(T)$ showing the diversity in electoral contexts. (b-g) Empirical scaled margin distributions $Q_{\widetilde{M}}(\widetilde{M})$ (open circles) compared with parameter-free RVM predictions (solid lines) for India, USA, South Korea, Canada, Japan, and Germany. The shaded regions represent prediction variability from multiple RVM realizations.

5.3.3.2 Scale-Independent Predictive Accuracy

The predictive power of the RVM extends across different electoral scales without requiring parameter adjustments. As shown in Figure 5.4 (b-g), the same model accurately predicts scaled margin distributions at both constituency-level (larger scale) and polling booth/county-level (smaller scale) for India, USA, and Canada. Despite turnout distributions that differ by orders of magnitude in scale and exhibit completely different shapes, the RVM maintains its predictive accuracy, confirming that the underlying statistical principles captured by the model are truly scale-invariant.

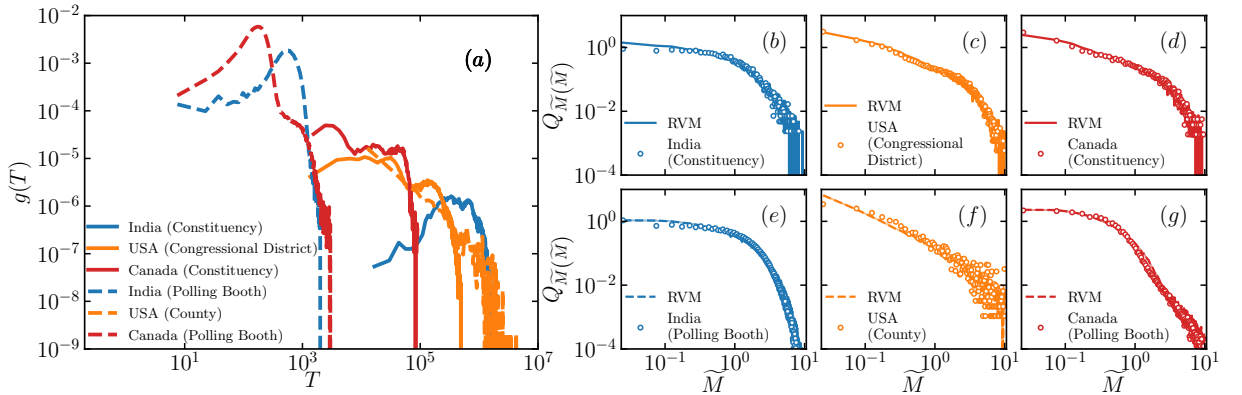


Figure 5.4: Scale-independent RVM predictions. (a) Turnout distributions $g(T)$ at two different electoral scales: dashed lines for smaller scales (polling booths/counties), solid lines for larger scales (constituencies/congressional districts). (b-g) Empirical $Q_{\widetilde{M}}(\widetilde{M})$ (open circles) and RVM predictions (lines) demonstrate excellent agreement across both scales despite vastly different turnout characteristics.

5.3.3.3 Comprehensive Validation Across All Countries

Figure 5.5 provides a comprehensive demonstration of the RVM’s predictive accuracy across our complete dataset of 32 countries. The remarkable agreement between empirical distributions (colored circles) and parameter-free RVM predictions (black lines) across such diverse electoral systems — spanning different continents, political cultures, and institutional arrangements — underscores the model’s robustness and the fundamental nature of the statistical principles it captures.

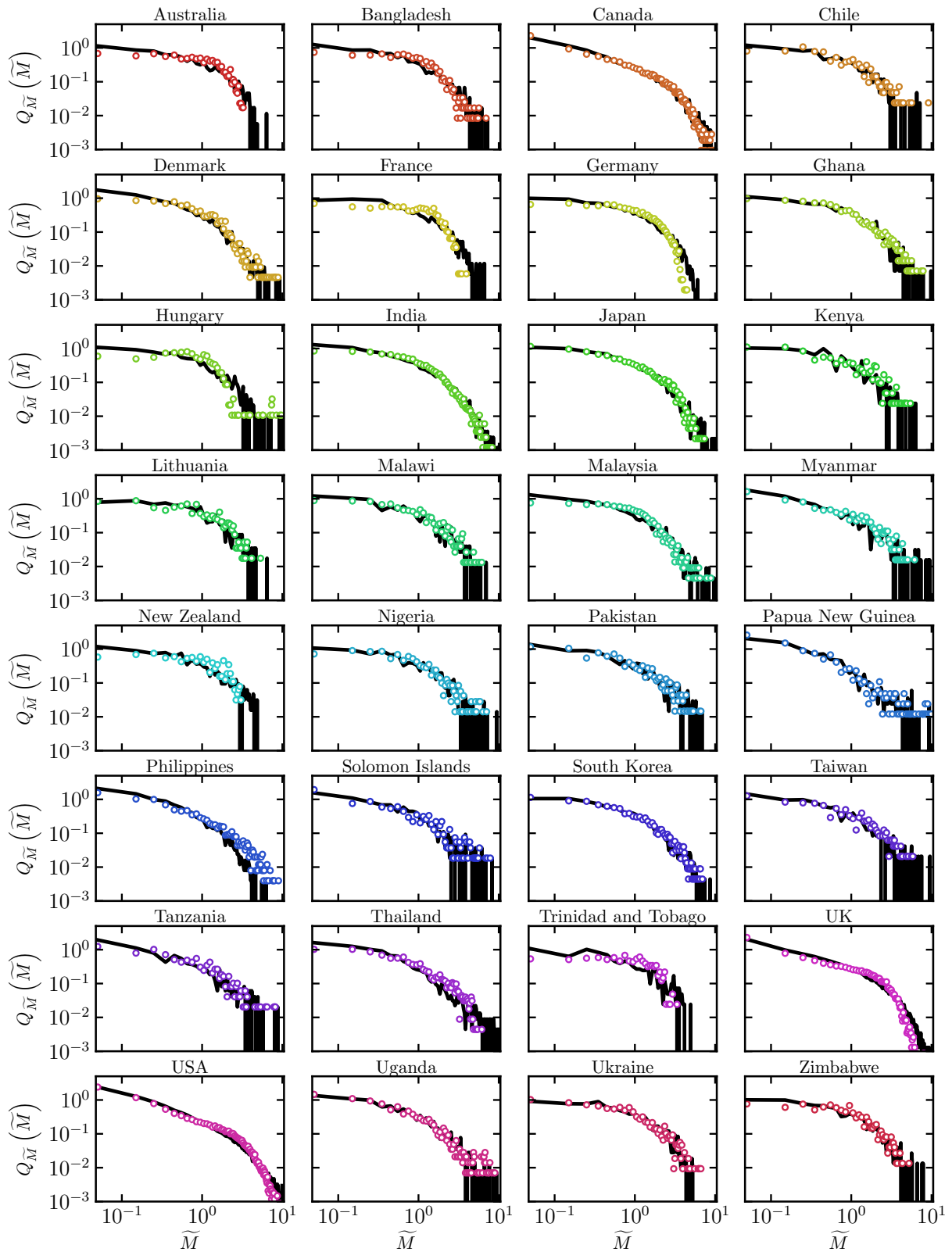


Figure 5.5: Comprehensive validation of RVM predictive accuracy. Empirical scaled margin distributions $Q_{\widetilde{M}}(\widetilde{M})$ (colored circles) compared with parameter-free RVM predictions (black solid lines) across all 32 countries in our dataset, demonstrating consistent predictive accuracy across diverse electoral systems.

5.4 Conclusion: The Power and Limitations of RVM

In this chapter, we have provided a comprehensive analysis of the Random Voting Model (RVM) from its first principles. We demonstrated how this elegantly simple model generates the universal distribution of scaled specific margins observed across diverse electoral systems worldwide. Through rigorous mathematical derivations, we showed that the model successfully predicts this universality without requiring any parameters beyond the turnout distribution and number of candidates.

Furthermore, we established that the RVM provides powerful insights into how turnout distributions shape margin distributions across different electoral contexts. Through both analytical solutions and simulations with various synthetic turnout distributions (Gaussian, exponential, power law, and uniform), we demonstrated that margin distributions inherit the tail behavior of their corresponding turnout distributions. This finding explains why electoral margin distributions can vary dramatically across countries while still adhering to the universal specific margin pattern.

The model's ability to predict scaled margin distributions from raw turnout data alone—without any adjustments or free parameters—is remarkable and represents a significant advance in our understanding of electoral statistics. It suggests that beneath the apparent complexity and diversity of electoral systems worldwide lies a fundamental statistical principle that governs competitive selection processes.

However, the RVM also has limitations. While it excellently predicts the shape and tail behavior of margin distributions, it struggles to reliably predict the mean margin. This necessitates scaling by empirical means when comparing model predictions to real-world data. Additionally, the model's simplified assumption of random voting does not account for strategic voting behavior, partisan affiliations, or other psychological and sociological factors that influence real elections.

Despite these limitations, the success of this minimal statistical model in capturing key universal features of electoral competition demonstrates the power of stochastic approaches in understanding complex social phenomena. It reveals that certain macroscopic patterns in electoral systems may be governed more by basic statistical principles than by the intricacies of voter psychology or electoral rules.

In the next chapter, we will build upon this foundation to explore prediction of several other key electoral statistics.

CHAPTER 6

Beyond Margins: Winner and Runner-up votes

Building on our exploration of the Random Voting Model in the previous chapter, we now extend our investigation to other key electoral statistics and their relationship with voter turnouts. While we established that the RVM successfully predicts the universal specific margin distribution and connects turnout distributions to margin distributions across different electoral contexts, a natural question arises: Can the distribution of other relevant electoral statistics be uncovered using voter turnout distributions?

To address this question effectively, we require large datasets covering a range of different electoral scales. India, the world's largest democracy, regularly conducts elections involving vast electorates (960 million in 2024), and its publicly available election data spans multiple decades and electoral scales. The diversity of India's linguistic and cultural landscape further adds to the complexities of its electoral outcomes, making it an excellent testing ground for assessing the robustness of the RVM framework.

In this chapter, using empirical data from Indian elections spanning several decades and vastly different electoral scales, we demonstrate a strong correlation between the distributions of votes received by winners and runner-ups and voter turnouts. Leveraging this correlation and the RVM, we analytically predict the scaled distributions of the votes secured by winners and runner-ups using the corresponding turnout distributions. This prediction remarkably holds good at all the electoral scales – from large parliamentary constituencies ($\sim 10^6$ voters) down to the smallest polling booth levels ($\sim 10^2 - 10^3$ voters). Further, we show a rather surprising scale invariance of the margin distributions, a characteristic typical of Indian elections.

6.1 The Effective Number of Candidates

While our previous analysis employed a fixed number of candidates ($n^c = 3$) for the Random Voting Model, here we refine our approach by introducing the concept of the effective number of candidates [98]. This metric, widely used in political science, captures the actual level of competition more accurately than the raw count of candidates on a ballot.

The effective number of candidates is defined as:

$${}^{(E)}n_i^c = \frac{1}{\sum_{k=1}^{{}^{(E)}n_i^c} (V_{ik}/T_i)^2}. \quad (6.1)$$

In large electoral exercises such as those in India, even though many candidates join the fray, a few corner most of the votes. For instance, if all the votes are garnered by just one candidate, then $V_{i1} = T_i$, and $V_{ij} = 0$ for $j = 2, \dots, {}^{(E)}n_i^c$. In this case, ${}^{(E)}n_i^c = 1$. However, if all the votes are split equally among two candidates, ${}^{(E)}n_i^c = 2$, thus, Eq. 6.1 captures the idea of an effective number of candidates in i -th electoral unit.

By averaging over all the electoral units, we obtain:

$${}^{(E)}\tilde{n}^c = \left[\frac{1}{N} \sum_{k=1}^N {}^{(E)}n_k^c \right], \quad (6.2)$$

where $[*]$ denotes the operation of extracting the closest integer value. And ${}^{(E)}\tilde{n}^c$ indicates the effective number of candidates for an entire election at different electoral scales.

From empirical data of Indian elections at different scales, we find ${}^{(E)}\tilde{n}^c = 2$ at the polling booth (PB) level for the General Elections. However, for all the other three cases of Assembly Constituency in General Elections (AC-GE), Parliamentary Constituency in General Elections (PC-GE), and Assembly Constituency in State Elections (AC-SE), we obtain ${}^{(E)}\tilde{n}^c = 3$. This insight allows us to adapt our modeling approach to better match the electoral reality at each scale.

6.2 Relationship Between Turnout and Vote Distributions

Depending on the electoral level considered, the winner and runner-up vote distributions have vastly different scales, with the winner vote distribution having wider support than the runner-up. However, when both distributions are scaled by their respective mean values (mean taken over all elections for which data is available), the winner and runner-up vote distributions – $Q_{\widetilde{V}_w}(\widetilde{V}_w)$ and $Q_{\widetilde{V}_r}(\widetilde{V}_r)$ – explicitly display a strong correlation with the corresponding scaled turnout distributions $Q_{\widetilde{T}}(\widetilde{T})$. Figure 6.1 shows this correlation for four different electoral scales in India.

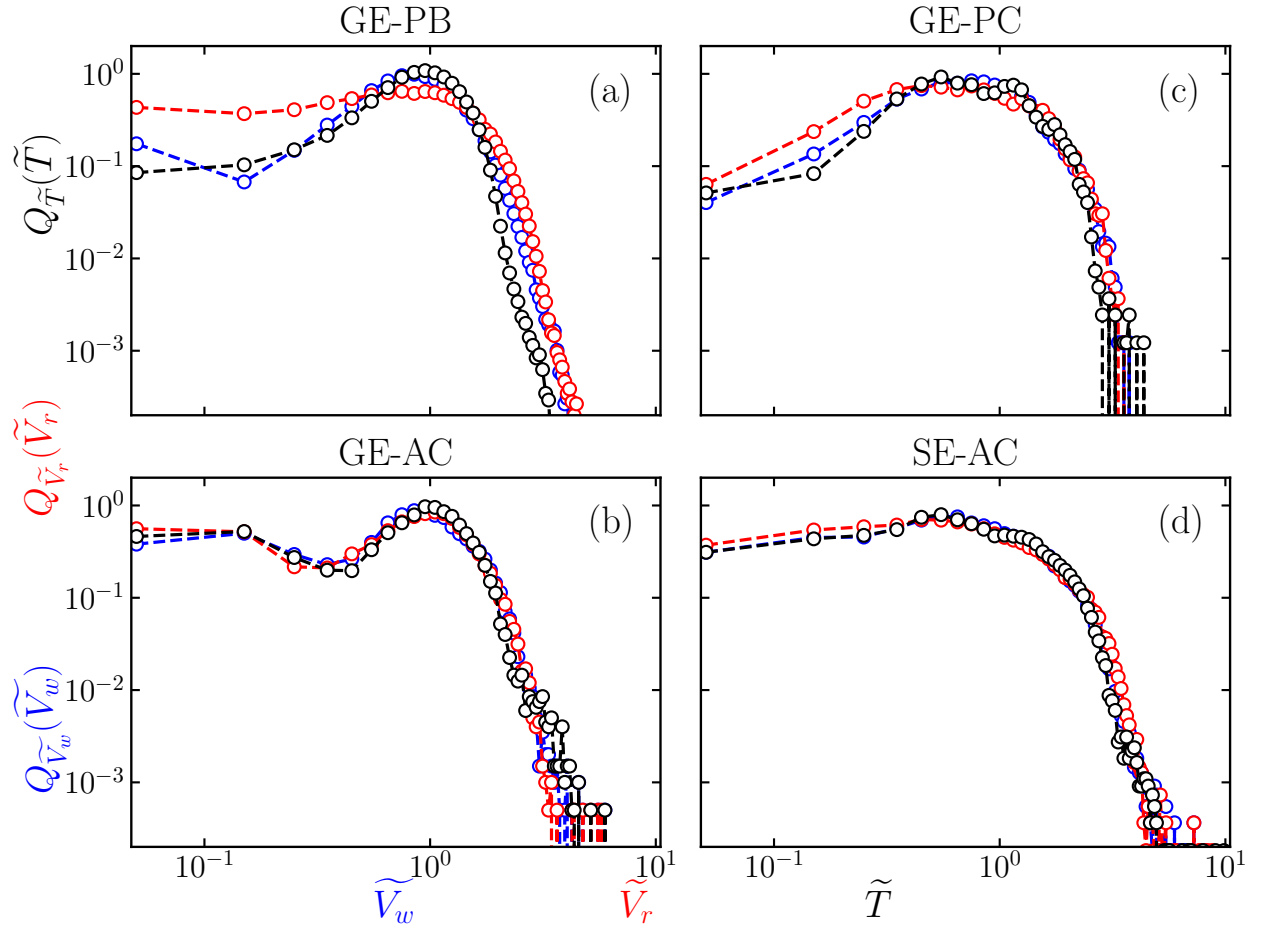


Figure 6.1: Winner, runner-up vote distributions, and turnout distributions, scaled by their respective means. Notably, at larger electoral scales (AC / PC), the winner and runner-up distributions mimic the corresponding turnout distribution.

Remarkably, at larger electoral scales (Parliamentary and Assembly constituencies), not only the tail but the entire scaled distributions of winner and runner-up votes mimic the corresponding scaled turnout distribution (panel (b) and (c) and (d) in Fig. 6.1). This strong correlation indicates that the turnout distribution contains crucial information about different election statistics and can be leveraged to predict the scaled vote distributions of the winner and the runner-up. To explore this possibility, we apply the Random Voting Model, which has already demonstrated effectiveness at predicting the scaled distribution of margins of victory.

6.3 Predicting Vote Distributions from Turnout Distributions

We now extend our analytical framework to derive the distributions of votes received by winners and runner-ups in the RVM.

6.3.1 Random Voting Model: a Quick Recap

In Random Voting Model, in the i -th electoral unit, electorates vote for the j -th candidate with a probability p_{ij} . These probabilities are assigned to the candidates as follows:

$$w_{ij} \sim \mathcal{U}(0, 1) \quad \text{and} \quad p_{ij} = \frac{w_{ij}}{\sum_k w_{ik}}, \text{ with } j = 1, 2 \dots n_i^c, \quad (6.3)$$

where $\mathcal{U}(0, 1)$ denotes a uniformly distributed random variable in $(0, 1)$ and n_i^c is the number of candidates in the i -th electoral unit.

6.3.2 Vote Share Distributions at Large Turnout Limit

For large turnout ($T \gg 1$), the votes received by the j -th candidate can be approximated as $V_j \approx p_j T$ (we remove the electoral unit index i for brevity). Consequently, the vote share is defined as:

$$v_j = V_j / T \text{ with } j = 1, 2, \dots, n^c. \quad (6.4)$$

Thus, in this limit, the vote share distribution is effectively the same as the distribution of p_j . Building on the order statistics framework introduced in the previous chapter, the winner's vote share v_w and runner-up's vote share v_r can be expressed as:

$$v_w = \frac{w_{(n^c)}^{n^c}}{\sum_{k=1}^{n^c} w_{(k)}^{n^c}} \quad \text{and} \quad v_r = \frac{w_{(n^c-1)}^{n^c}}{\sum_{k=1}^{n^c} w_{(k)}^{n^c}}. \quad (6.5)$$

6.3.3 Random Voting Model with two candidates

In the following sections, we derive analytical expressions for the vote share distributions of winner and runner-up candidates. We begin with the simpler two-candidate case before extending to the more complex three-candidate scenario. These mathematical derivations will allow us to predict the shape of vote distributions based solely on turnout data.

In the two-candidate Random Voting Model, we have $n = n^c = 2$ and $w_j \sim \mathcal{U}(0, 1)$. Hence, the joint probability distribution of all the order statistics have the following form,

$$\mathbb{P}(w_{(1)}, w_{(2)}) = 2! = 2; \text{ with } 0 < w_{(1)} < w_{(2)} < 1, \quad (6.6)$$

and $\mathbb{P}(w_{(1)}, w_{(2)}) = 0$ otherwise, with the following normalization:

$$\int_0^1 dw_{(2)} \int_0^{w_{(2)}} 2dw_{(1)} = 1. \quad (6.7)$$

6.3.3.1 Winner vote share distribution

From the joint probability distribution of all the order statistics (Eq. 6.6), the approximate vote share distribution of the winner can be obtained as,

$$\begin{aligned} P_{v_w}(v_w) &= 2 \int_0^1 dw_{(2)} \int_0^{w_{(2)}} \delta\left(v_w - \frac{w_{(2)}}{w_{(1)} + w_{(2)}}\right) dw_{(1)}, \\ &= 2 \int_0^1 \frac{2w_{(2)}}{v_w^2} \mathbb{1}_{1/2 \leq v_w < 1} dw_{(2)}, \end{aligned} \quad (6.8)$$

or,

$$P_{v_w}(v_w) = \begin{cases} \frac{1}{v_w^2} & \text{if } \frac{1}{2} \leq v_w < 1 \\ 0, & \text{otherwise.} \end{cases} \quad (6.9)$$

$$(6.10)$$

6.3.3.2 Runner-up vote share distribution

We can similarly calculate the probability density function of the runner-up vote share as the following,

$$\begin{aligned} P_{v_r}(v_r) &= 2 \int_0^1 dw_{(2)} \int_0^{w_{(2)}} \delta\left(v_r - \frac{w_{(1)}}{w_{(1)} + w_{(2)}}\right) dw_{(1)}, \\ &= 2 \int_0^1 \frac{2w_{(2)}}{(1 - v_r)^2} \mathbb{1}_{0 < v_r < 1/2} dw_{(2)}, \end{aligned} \quad (6.11)$$

or,

$$P_{v_r}(v_r) = \begin{cases} \frac{1}{(1 - v_r)^2} & \text{if } 0 < v_r < \frac{1}{2} \\ 0, & \text{otherwise.} \end{cases} \quad (6.12)$$

$$(6.13)$$

6.3.4 Random Voting Model with three candidates

In the three-candidate Random Voting Model, we have $n = n^c = 3$ and $w_j \sim \mathcal{U}(0, 1)$. Then, the joint probability distribution of all the order statistics is,

$$\mathbb{P}(w_{(1)}, w_{(2)}, w_{(3)}) = 3! = 6; \text{ with } 0 < w_{(1)} < w_{(2)} < w_{(3)} < 1, \quad (6.14)$$

and $\mathbb{P}(w_{(1)}, w_{(2)}, w_{(3)}) = 0$ otherwise, with the following normalization:

$$\int_0^1 dw_{(3)} \int_0^{w_{(3)}} dw_{(2)} \int_0^{w_{(2)}} 6dw_{(1)} = 1. \quad (6.15)$$

6.3.4.1 Winner vote share distribution

From the joint probability distribution of all the order statistics, we calculate the approximate probability density function of the winner vote share $v_w = V_w/T$ as follows,

$$\begin{aligned} P_{v_w}(v_w) &= 6 \int_0^1 dw_{(3)} \int_0^{w_{(3)}} dw_{(2)} \int_0^{w_{(2)}} \delta\left(v_w - \frac{w_{(3)}}{w_{(1)} + w_{(2)} + w_{(3)}}\right) dw_{(1)}, \\ &= 6 \int_0^1 dw_{(3)} \int_0^{w_{(3)}} \frac{w_{(3)}}{v_w^2} \mathbb{1}_{0 < \frac{w_{(3)} - v_w (w_{(2)} + w_{(3)})}{v_w} < w_{(2)}} dw_{(2)}, \end{aligned} \quad (6.16)$$

or,

$$P_{v_w} = \begin{cases} 6 \int_0^1 w_{(3)}^2 \frac{3v_w - 1}{2v_w^3} dw_{(3)}, & \text{if } \frac{1}{3} < v_w \leq \frac{1}{2} \\ 0, & \text{otherwise.} \end{cases} \quad (6.17)$$

$$P_{v_w} = \begin{cases} 6 \int_0^1 w_{(3)}^2 \frac{1 - v_w}{2v_w^3} dw_{(3)}, & \text{if } \frac{1}{2} < v_w \leq 1 \\ 0, & \text{otherwise.} \end{cases} \quad (6.18)$$

$$P_{v_w} = \begin{cases} 0, & \text{otherwise.} \end{cases} \quad (6.19)$$

Finally, after performing the integral, we get

$$P_{v_w} = \begin{cases} \frac{3v_w - 1}{v_w^3} & \text{if } \frac{1}{3} < v_w \leq \frac{1}{2} \\ 0, & \text{otherwise.} \end{cases} \quad (6.20)$$

$$P_{v_w} = \begin{cases} \frac{1 - v_w}{v_w^3}, & \text{if } \frac{1}{2} < v_w < 1 \\ 0, & \text{otherwise.} \end{cases} \quad (6.21)$$

$$P_{v_w} = \begin{cases} 0, & \text{otherwise.} \end{cases} \quad (6.22)$$

6.3.4.2 Runner-up vote share distribution

Similarly, the probability density function of the runner-up vote share $v_r = V_r/T$ can be obtained as follows,

$$\begin{aligned} P_{v_r}(v_w) &= 6 \int_0^1 dw_{(3)} \int_0^{w_{(3)}} dw_{(2)} \int_0^{w_{(2)}} \delta\left(v_r - \frac{w_{(2)}}{w_{(1)} + w_{(2)} + w_{(3)}}\right) dw_{(1)}, \\ &= 6 \int_0^1 dw_{(3)} \int_0^{w_{(3)}} \frac{w_{(2)}}{v_r^2} \mathbb{1}_{0 < (1/v_r - 1)w_{(2)} - w_{(3)} < w_{(2)}} dw_{(2)}, \end{aligned} \quad (6.23)$$

or,

$$P_{v_r}(v_r) = \begin{cases} 6 \int_0^1 w_{(3)}^2 \frac{v_r(2 - 3v_r)}{2(1 - v_r)^2(1 - 2v_r)^2} dw_{(3)}, & \text{if } 0 < v_r \leq \frac{1}{3} \end{cases} \quad (6.24)$$

$$P_{v_r}(v_r) = \begin{cases} 6 \int_0^1 w_{(3)}^2 \frac{1 - 2v_r}{2v_r^2(1 - v_r)^2} dw_{(3)}, & \text{if } \frac{1}{3} < v_r < \frac{1}{2} \end{cases} \quad (6.25)$$

$$P_{v_r}(v_r) = 0, \text{ otherwise.} \quad (6.26)$$

Finally, after performing the integral, we get

$$P_{v_r}(v_r) = \begin{cases} \frac{v_r(2 - 3v_r)}{(1 - v_r)^2(1 - 2v_r)^2} & \text{if } 0 < v_r \leq \frac{1}{3} \end{cases} \quad (6.27)$$

$$P_{v_r}(v_r) = \begin{cases} \frac{1 - 2v_r}{v_r^2(1 - v_r)^2}, & \text{if } \frac{1}{3} < v_r < \frac{1}{2} \end{cases} \quad (6.28)$$

$$P_{v_r}(v_r) = 0, \text{ otherwise.} \quad (6.29)$$

6.3.5 Calculating the *scaled* distributions

The winner and runner-up vote shares and specific margins are random variables scaled by the voter turnout T . However, through a simple change of variable, $Y = yT$, we can obtain the conditional distributions of the unscaled variables as,

$$\mathcal{P}(Y|T) = \frac{1}{T} P_y(Y/T), \quad (6.30)$$

where y can be v_w , v_r , and μ and Y represents unscaled variables V_w , V_r , and M respectively. The distribution of Y for an arbitrary turnout distribution $g(T)$ can be obtained as,

$$Q_Y(Y) = \int g(T) \mathcal{P}(Y|T) dT, \quad (6.31)$$

with $\langle Y \rangle$ defined as,

$$\langle Y \rangle = \int Y Q_Y(Y) dY. \quad (6.32)$$

Finally the distribution of *scaled* Y , defined as $\tilde{Y} = Y/\langle Y \rangle$, can be obtained as follows,

$$Q_{\tilde{Y}}(\tilde{Y}) = \langle Y \rangle Q_Y(\tilde{Y}\langle Y \rangle) \quad (6.33)$$

Again, the dummy random variable Y can be either, V_w or V_r .

6.4 Empirical Validation across Electoral Scales

Having derived the analytical expressions for vote share distributions, we now turn to testing these predictions against real-world election data. This validation process will demonstrate how well our theoretical framework captures the essential features of electoral outcomes across different scales.

To validate our analytical framework, we compare the predicted distributions against empirical data from four different electoral scales in India:

1. Parliamentary Constituency level in General Elections (GE-PC): $\sim 10^6$ voters
2. Assembly Constituency level in General Elections (GE-AC): $\sim 10^5$ voters
3. Polling Booth level in General Elections (GE-PB): $\sim 10^3$ voters
4. Assembly Constituency level in State Elections (SE-AC): $\sim 10^5$ voters

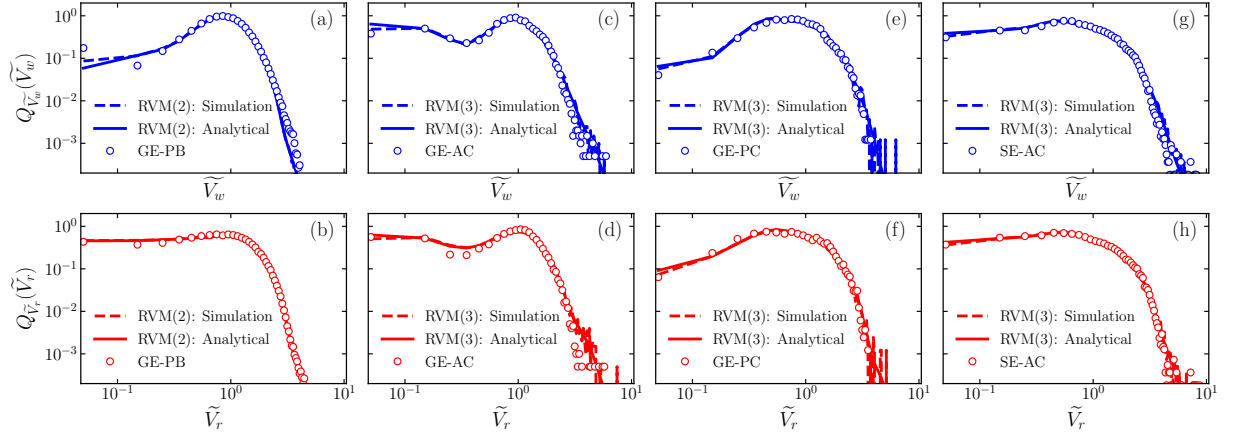


Figure 6.2: Winner and runner-up vote distributions scaled by their respective means. Panels (a, b), (c, d), and (e, f) depict, respectively, the scaled winner and runner-up vote distribution at the polling booth, assembly constituency, and parliamentary constituency level for Indian general elections. Panels (g, h) correspond to the distributions for the state elections at the assembly constituency level. The analytical predictions (solid lines) are in remarkable agreement with the empirical distributions (open circle). Predictions from RVM simulations (dashed line) closely follow the analytical curves. Note particularly the power-law behavior in the tails ($\tilde{V} \gg 1$) across all scales, and the distinct profiles at small values ($\tilde{V} \ll 1$) that vary with the effective number of candidates.

Using the empirical turnout distribution $g(T)$ from election data, Eq. 6.31 is numerically integrated. The resulting distribution is then scaled using Eq. 6.33 to obtain the scaled distributions for the winner and runner-up vote shares, $Q_{\tilde{V}_w}(\tilde{V}_w)$ and $Q_{\tilde{V}_r}(\tilde{V}_r)$, respectively. As demonstrated in Fig. 6.2, the analytical prediction (solid lines) is remarkably consistent with the empirical vote share distributions. The predictions from RVM simulations, which use the raw turnout data and $n^c = {}^{(E)}\tilde{n}^c$ as inputs, closely follow the analytical distributions in Fig. 6.2.

The scaled distributions of winner and runner-up votes depicted across all electoral scales, in Fig. 6.2, typically exhibit a power-law behavior in the tails for $\tilde{V}_w, \tilde{V}_r \gg 1$. Conversely, for $\tilde{V}_w, \tilde{V}_r \ll 1$, the distributions display different profiles. Remarkably, these differences are well captured by RVM predictions: RVM ($T, 2$) accurately predicts distribution at the GE-PB level, while RVM ($T, 3$) closely matches the distributions at the GE-AC, GE-PC, and SE-AC levels. Hence, the effective number of candidates (Eq. 6.1) and the turnout distribution $g(T)$, when used within the RVM framework, successfully predict the winner and runner-up vote share distributions across distinct electoral scales.

6.5 Scale Invariance of Margin Distributions in Indian Elections

Building on our analysis of specific margins $\mu = M/T$ from the previous chapter, we now examine the behavior of the scaled margin distributions $Q_{\widetilde{M}}(\widetilde{M})$ across different electoral scales in India.

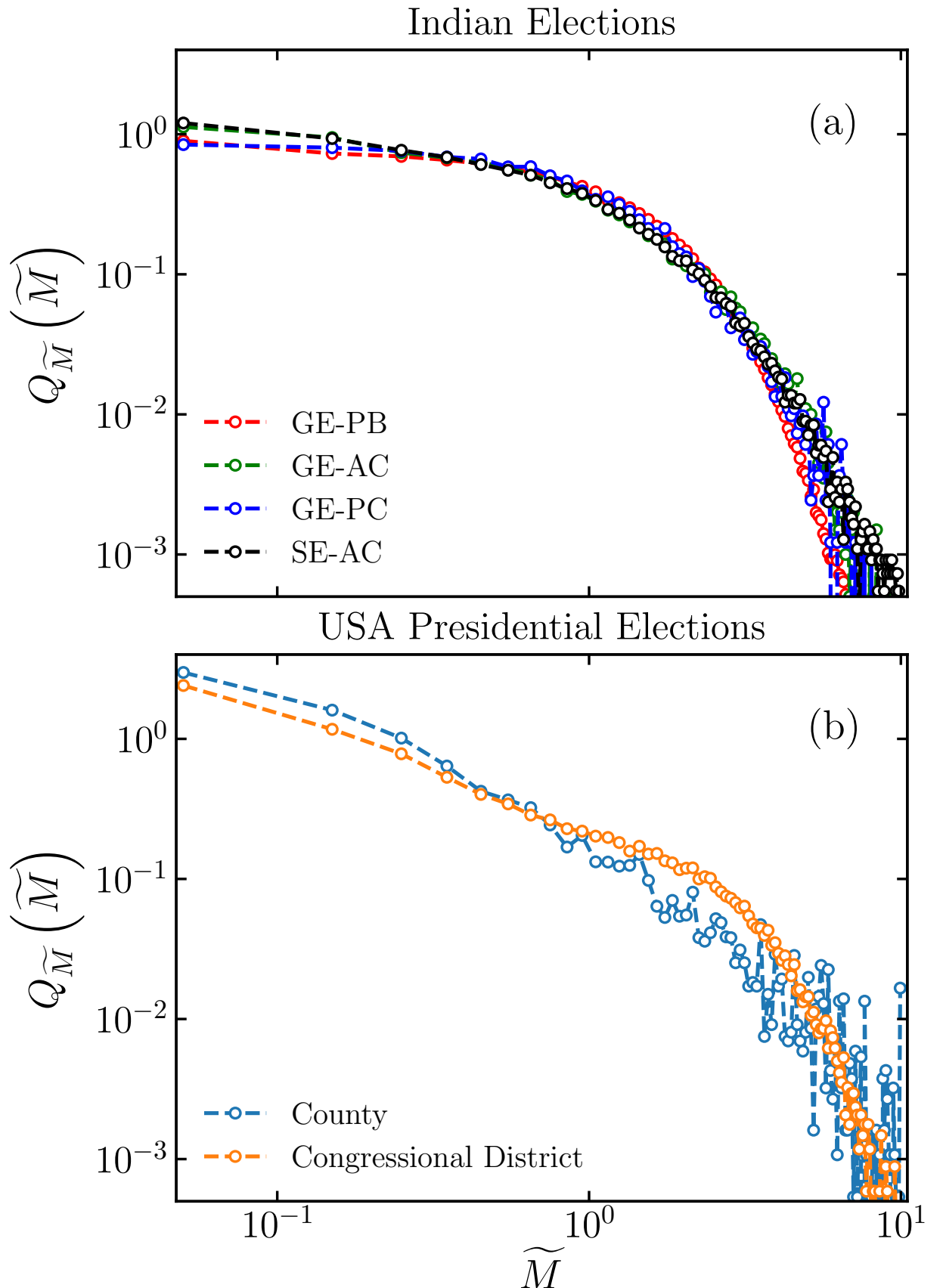


Figure 6.3: Margin distributions scaled by their respective means. (a) Data collapse in the scaled margin distributions of Indian elections at four electoral scales. Note how despite the vastly different electoral sizes (from $\sim 10^2$ to $\sim 10^6$ voters), the distributions align remarkably well. (b) In contrast, such collapse is absent in the election data from the USA, where county and district level distributions differ significantly.

Remarkably, as demonstrated in Fig. 6.3 (a), the scaled distributions for the margin for Indian elections at four different scales (GE-PB, GE-AC, GE-PC, and SE-AC) collapse onto a single curve. This data collapse is a direct consequence of the similarity in tail behavior in the corresponding turnout distributions. This appears to be a characteristic feature of Indian elections.

For instance, scaled margin distributions from US elections at the County and Congressional district levels do not exhibit such a collapse (Fig. 6.3 (b)). This finding highlights a unique characteristic of the Indian electoral system that deserves further investigation.

6.6 Conclusion: Turnout Distributions as Electoral Predictors

In summary, this chapter has demonstrated that voter turnout distributions are not merely indicators of public trust and interest in the electoral process, but they also encode crucial information about several key election statistics. The Random Voting Model, enhanced with the concept of effective number of candidates, provides a powerful framework for predicting various electoral statistics from turnout distributions alone.

Our analysis reveals that voter turnout distributions strongly correlate with winner and runner-up vote distributions, especially at larger electoral scales. This correlation is particularly evident in the remarkable agreement between the analytical predictions from our model and the empirical data. The RVM, when parameterized with the appropriate effective number of candidates ($n^c = 2$ for polling booth level, $n^c = 3$ for constituency levels), accurately predicts the scaled distributions of winner and runner-up votes across different electoral contexts.

Perhaps most striking among our findings is that Indian elections exhibit a unique scale invariance in margin distributions, with scaled margin distributions collapsing onto a single curve across vastly different electoral scales. This phenomenon, not observed in many other democratic systems including the United States, highlights distinctive characteristics of the Indian electoral landscape. Furthermore, the universality of the scaled specific margin distribution is confirmed across multiple electoral scales within India, reinforcing the robustness of our analytical framework.

These findings deepen our understanding of electoral statistics and their relationship with voter turnouts. The predictive power of the RVM framework, using only turnout data and the effective number of candidates as inputs, provides a valuable tool for electoral analysis and could potentially aid in identifying anomalies or irregularities in electoral processes.

As we move to the next chapter, we will explore the practical applications of these insights,

focusing on designing interventions and developing methods to flag electoral malpractice based on deviations from the expected statistical patterns.

Bibliography

- [1] S. Galam. *Sociophysics: A Physicist's Modeling of Psycho-political Phenomena*. Understanding Complex Systems. Springer New York, 2012.
- [2] Shannon C McGregor. Social media as public opinion: How journalists use social media to represent public opinion. *Journalism*, 20(8):1070–1086, 2019.
- [3] Serge Galam, Yuval Gefen, and Yonathan Shapir. Sociophysics: A new approach of sociological collective behaviour. i. mean-behaviour description of a strike. *Journal of Mathematical Sociology*, 9(1):1–13, 1982.
- [4] Serge Galam and Serge Moscovici. Towards a theory of collective phenomena: Consensus and attitude changes in groups. *European Journal of Social Psychology*, 21(1):49–74, 1991.
- [5] Charles G Lord, Lee Ross, and Mark R Lepper. Biased assimilation and attitude polarization: The effects of prior theories on subsequently considered evidence. *Journal of personality and social psychology*, 37(11):2098, 1979.
- [6] Paul DiMaggio, John Evans, and Bethany Bryson. Have american's social attitudes become more polarized? *American journal of Sociology*, 102(3):690–755, 1996.
- [7] Delia Baldassarri and Andrew Gelman. Partisans without constraint: Political polarization and trends in american public opinion. *American Journal of Sociology*, 114(2):408–446, 2008.
- [8] R Kelly Garrett. Echo chambers online?: Politically motivated selective exposure among internet news users. *Journal of computer-mediated communication*, 14(2):265–285, 2009.
- [9] Michela Del Vicario, Gianna Vivaldo, Alessandro Bessi, Fabiana Zollo, Antonio Scala, Guido Caldarelli, and Walter Quattrociocchi. Echo chambers: Emotional contagion and group polarization on facebook. *Scientific reports*, 6(1):37825, 2016.
- [10] Wesley Cota, Silvio C Ferreira, Romualdo Pastor-Satorras, and Michele Starnini. Quantifying echo chamber effects in information spreading over political communication networks. *EPJ Data Science*, 8(1):35, 2019.

BIBLIOGRAPHY

- [11] Kiran Garimella, Gianmarco De Francisci Morales, Aristides Gionis, and Michael Mathioudakis. Political discourse on social media: Echo chambers, gatekeepers, and the price of bipartisanship. In *Proceedings of the 2018 world wide web conference*, pages 913–922, 2018.
- [12] Matteo Cinelli, Gianmarco De Francisci Morales, Alessandro Galeazzi, Walter Quattrociocchi, and Michele Starnini. The echo chamber effect on social media. *Proceedings of the National Academy of Sciences*, 118(9):e2023301118, 2021.
- [13] Fernando P Santos, Yphtach Lelkes, and Simon A Levin. Link recommendation algorithms and dynamics of polarization in online social networks. *Proceedings of the National Academy of Sciences*, 118(50):e2102141118, 2021.
- [14] Morris H DeGroot. Reaching a consensus. *Journal of the American Statistical association*, 69(345):118–121, 1974.
- [15] Richard A Holley and Thomas M Liggett. Ergodic theorems for weakly interacting infinite systems and the voter model. *The annals of probability*, pages 643–663, 1975.
- [16] Sidney Redner. Reality-inspired voter models: A mini-review. *Comptes Rendus Physique*, 20(4):275–292, 2019.
- [17] Katarzyna Sznajd-Weron and Józef Sznajd. Opinion evolution in closed community. *International Journal of Modern Physics C*, 11(06):1157–1165, 2000.
- [18] Katarzyna Sznajd-Weron, Józef Sznajd, and Tomasz Weron. A review on the sznajd model—20 years after. *Physica A: Statistical Mechanics and its Applications*, 565:125537, 2021.
- [19] Robert Axelrod. The dissemination of culture: A model with local convergence and global polarization. *Journal of conflict resolution*, 41(2):203–226, 1997.
- [20] Serge Galam. Minority opinion spreading in random geometry. *The European Physical Journal B-Condensed Matter and Complex Systems*, 25:403–406, 2002.
- [21] Serge Galam and Frans Jacobs. The role of inflexible minorities in the breaking of democratic opinion dynamics. *Physica A: Statistical Mechanics and its Applications*, 381:366–376, 2007.

- [22] Serge Galam. Stubbornness as an unfortunate key to win a public debate: an illustration from sociophysics. *Mind & Society*, 15:117–130, 2016.
- [23] Serge Galam. Collective beliefs versus individual inflexibility: The unavoidable biases of a public debate. *Physica A: Statistical Mechanics and its Applications*, 390(17):3036–3054, 2011.
- [24] Guillaume Deffuant, David Neau, Frederic Amblard, and Gérard Weisbuch. Mixing beliefs among interacting agents. *Advances in Complex Systems*, 3(01n04):87–98, 2000.
- [25] Hegselmann Rainer and Ulrich Krause. Opinion dynamics and bounded confidence: models, analysis and simulation. 2002.
- [26] Fabian Baumann, Philipp Lorenz-Spreen, Igor M Sokolov, and Michele Starnini. Modeling echo chambers and polarization dynamics in social networks. *Physical Review Letters*, 124(4):048301, 2020.
- [27] Fabian Baumann, Philipp Lorenz-Spreen, Igor M Sokolov, and Michele Starnini. Emergence of polarized ideological opinions in multidimensional topic spaces. *Physical Review X*, 11(1):011012, 2021.
- [28] Kazutoshi Sasahara, Wen Chen, Hao Peng, Giovanni Luca Ciampaglia, Alessandro Flammini, and Filippo Menczer. Social influence and unfollowing accelerate the emergence of echo chambers. *Journal of Computational Social Science*, 4(1):381–402, 2021.
- [29] Vítor V Vasconcelos, Sara M Constantino, Astrid Dannenberg, Marcel Lumkowsky, Elke Weber, and Simon Levin. Segregation and clustering of preferences erode socially beneficial coordination. *Proceedings of the National Academy of Sciences*, 118(50):e2102153118, 2021.
- [30] Petter Törnberg. Echo chambers and viral misinformation: Modeling fake news as complex contagion. *PLoS one*, 13(9):e0203958, 2018.
- [31] Michela Del Vicario, Alessandro Bessi, Fabiana Zollo, Fabio Petroni, Antonio Scala, Guido Caldarelli, H Eugene Stanley, and Walter Quattrociocchi. The spreading of misinformation online. *Proceedings of the national academy of Sciences*, 113(3):554–559, 2016.

BIBLIOGRAPHY

- [32] Philip W Anderson. More is different: Broken symmetry and the nature of the hierarchical structure of science. *Science*, 177(4047):393–396, 1972.
- [33] Steven Strogatz, Sara Walker, Julia M Yeomans, Corina Tarnita, Elsa Arcaute, Manlio De Domenico, Oriol Artíme, and Kwang-Il Goh. Fifty years of ‘more is different’. *Nature Reviews Physics*, 4(8):508–510, 2022.
- [34] Claudio Castellano, Santo Fortunato, and Vittorio Loreto. Statistical physics of social dynamics. *Rev. Mod. Phys.*, 81:591–646, May 2009.
- [35] Arkadiusz Jedrzejewski and Katarzyna Sznajd Weron. Statistical physics of opinion formation: Is it a spoof? *Comptes Rendus Physique*, 20(4):244–261, 2019.
- [36] Maxi San Miguel and Raul Toral. Introduction to the chaos focus issue on the dynamics of social systems. *Chaos: An Interdisciplinary Journal of Nonlinear Science*, 30(12), 2020. See all the papers that are part of this special issue.
- [37] Serge Galam. *Sociophysics: A Physicist’s Modeling of Psycho-political Phenomena*. Springer New York, NY, 2012.
- [38] Steven J. Brams. *Mathematics and Democracy : Designing better voting and fair-division procedures*. Princeton University Press, Princeton, 2008.
- [39] S Fortunato. Santo fortunato· michael macy· sidney redner. *J Stat Phys*, 151:1–8, 2013.
- [40] Jean-Philippe Bouchaud. From statistical physics to social sciences: the pitfalls of multidisciplinarity. *Journal of Physics: Complexity*, 4(4):041001, dec 2023.
- [41] Parongama Sen and Bikas K Chakrabarti. *Sociophysics: an introduction*. OUP, Oxford, 2014.
- [42] Matjaž Perc, Jillian J. Jordan, David G. Rand, Zhen Wang, Stefano Boccaletti, and Attila Szolnoki. Statistical physics of human cooperation. *Physics Reports*, 687:1–51, 2017.
- [43] Marko Jusup, Petter Holme, Kiyoshi Kanazawa, Misako Takayasu, Ivan Romić, Zhen Wang, Sunčana Geček, Tomislav Lipić, Boris Podobnik, Lin Wang, Wei Luo, Tin Klanjšček, Jingfang Fan, Stefano Boccaletti, and Matjaž Perc. Social physics. *Physics Reports*, 948:1–148, 2022.

- [44] Sidney Redner. Reality-inspired voter models: A mini-review. *Comptes Rendus Physique*, 20(4):275–292, 2019.
- [45] F. Reif. *Fundamentals of Statistical and Thermal Physics*. McGraw Hill, Tokyo, 1965.
- [46] Álvaro Corral. Long-term clustering, scaling, and universality in the temporal occurrence of earthquakes. *Phys. Rev. Lett.*, 92:108501, Mar 2004.
- [47] Álvaro Corral. Universal earthquake-occurrence jumps, correlations with time, and anomalous diffusion. *Phys. Rev. Lett.*, 97:178501, Oct 2006.
- [48] Vasiliki Plerou, Parameswaran Gopikrishnan, Bernd Rosenow, Luís A. Nunes Amaral, and H. Eugene Stanley. Universal and nonuniversal properties of cross correlations in financial time series. *Phys. Rev. Lett.*, 83:1471–1474, Aug 1999.
- [49] R. N. Costa Filho, M. P. Almeida, J. S. Andrade, and J. E. Moreira. Scaling behavior in a proportional voting process. *Phys. Rev. E*, 60:1067–1068, Jul 1999.
- [50] Santo Fortunato and Claudio Castellano. Scaling and universality in proportional elections. *Phys. Rev. Lett.*, 99:138701, Sep 2007.
- [51] C. Borghesi and J.-P. Bouchaud. Spatial correlations in vote statistics: a diffusive field model for decision-making. *Eur. Phys. J. B*, 75(3):395–404, June 2010.
- [52] MC Mantovani, HV Ribeiro, MV Moro, S Picoli, and RS Mendes. Scaling laws and universality in the choice of election candidates. *Europhysics Letters*, 96(4):48001, 2011.
- [53] Eszter Bokányi, Zoltán Szállási, and Gábor Vattay. Universal scaling laws in metro area election results. *PLOS ONE*, 13(2):1–11, 02 2018.
- [54] Arnab Chatterjee, Marija Mitrović, and Santo Fortunato. Universality in voting behavior: an empirical analysis. *Scientific reports*, 3(1):1049, 2013.
- [55] Volker Hösel, Johannes Müller, and Aurelien Tellier. Universality of neutral models: Decision process in politics. *Palgrave Communications*, 5(1):1–8, 2019.
- [56] Aleksejus Kononovicius. Modeling of the parties’ vote share distributions. *Acta Physica Polonica A*, 133(6):1450, 2018.

BIBLIOGRAPHY

- [57] Aleksejus Kononovicius. Compartmental voter model. *Journal of Statistical Mechanics: Theory and Experiment*, 2019(10):103402, oct 2019.
- [58] Angelo Mondaini Calvão, Nuno Crokidakis, and Celia Anteneodo. Stylized facts in brazilian vote distributions. *PLOS ONE*, 10(9):1–20, 09 2015.
- [59] Christian Borges, Jean-Claude Raynal, and Jean-Philippe Bouchaud. Election turnout statistics in many countries: Similarities, differences, and a diffusive field model for decision-making. *PLOS ONE*, 7(5):1–12, 05 2012.
- [60] Juan Fernández-Gracia, Krzysztof Suchecki, José J. Ramasco, Maxi San Miguel, and Víctor M. Eguíluz. Is the voter model a model for voters? *Phys. Rev. Lett.*, 112:158701, Apr 2014.
- [61] Dan Braha and Marcus A. M. de Aguiar. Voting contagion: Modeling and analysis of a century of u.s. presidential elections. *PLOS ONE*, 12(5):1–30, 05 2017.
- [62] Jérôme Michaud, Ilkka H Mäkinen, Attila Szilva, and Emil Frisk. A spatial analysis of parliamentary elections in sweden 1985–2018. *Applied Network Science*, 6(1):1–28, 2021.
- [63] Shintaro Mori, Masato Hisakado, and Kazuaki Nakayama. Voter model on networks and the multivariate beta distribution. *Phys. Rev. E*, 99:052307, May 2019.
- [64] Gary C Jacobson. The marginals never vanished: Incumbency and competition in elections to the us house of representatives, 1952-82. *American Journal of Political Science*, pages 126–141, 1987.
- [65] Stewart JH McCann. Threatening times,” strong” presidential popular vote winners, and the victory margin, 1824–1964. *Journal of personality and social psychology*, 73(1):160, 1997.
- [66] Casey B Mulligan and Charles G Hunter. The empirical frequency of a pivotal vote. *Public Choice*, 116(1):31–54, 2003.
- [67] Thomas R Magrino, Ronald L Rivest, and Emily Shen. Computing the margin of victory in {IRV} elections. In *2011 Electronic Voting Technology Workshop/Workshop on Trustworthy Elections (EVT/WOTE 11)*, 2011.
- [68] Lirong Xia. Computing the margin of victory for various voting rules. In *Proceedings of the 13th ACM conference on electronic commerce*, pages 982–999, 2012.

- [69] Arnab Bhattacharyya and Palash Dey. Predicting winner and estimating margin of victory in elections using sampling. *Artificial Intelligence*, 296:103476, 2021.
- [70] Election data of india. <https://www.eci.gov.in>.
- [71] Constituency-level elections archive [data file and codebook]. <http://www.electiondataarchive.org>.
- [72] Election data of canada. <https://www.elections.ca>.
- [73] MIT Election Data and Science Lab. County Presidential Election Returns 2000-2020, 2018.
- [74] Glenn Brigaldino. Elections in the imperial periphery: Ethiopia hijacked. *Review of African political economy*, 38(128):327–334, 2011.
- [75] Matthew Frear. The parliamentary elections in belarus, september 2012. *Electoral Studies*, 33(1):350–353, 2014.
- [76] Report of organization for security and co-operation in europe (osce). <https://www.osce.org/odihr/elections/belarus>, 2020.
- [77] Arkadiusz Czołek and Julia Kołodziejska. Belarusian parliamentary election in 2019. *The Copernicus Journal of Political Studies*, (1):81–93, 2021.
- [78] Sofie Bedford. The 2020 presidential election in belarus: Erosion of authoritarian stability and re-politicization of society. *Nationalities Papers*, 49(5):808–819, 2021.
- [79] Peter Klimek, Yuri Yegorov, Rudolf Hanel, and Stefan Thurner. Statistical detection of systematic election irregularities. *Proceedings of the National Academy of Sciences*, 109(41):16469–16473, 2012.
- [80] Raúl Jimenez, Manuel Hidalgo, and Peter Klimek. Testing for voter rigging in small polling stations. *Science advances*, 3(6):e1602363, 2017.
- [81] David G Myers and Helmut Lamm. The group polarization phenomenon. *Psychological bulletin*, 83(4):602, 1976.
- [82] Daniel J Isenberg. Group polarization: A critical review and meta-analysis. *Journal of personality and social psychology*, 50(6):1141, 1986.

BIBLIOGRAPHY

- [83] Nicola Perra, Bruno Gonçalves, Romualdo Pastor-Satorras, and Alessandro Vespignani. Activity driven modeling of time varying networks. *Scientific reports*, 2(1):469, 2012.
- [84] Michele Starnini and Romualdo Pastor-Satorras. Topological properties of a time-integrated activity-driven network. *Physical Review E*, 87(6):062807, 2013.
- [85] Antoine Moinet, Michele Starnini, and Romualdo Pastor-Satorras. Burstiness and aging in social temporal networks. *Physical review letters*, 114(10):108701, 2015.
- [86] Suyu Liu, Nicola Perra, Márton Karsai, and Alessandro Vespignani. Controlling contagion processes in activity driven networks. *Physical review letters*, 112(11):118702, 2014.
- [87] Christopher Brian Currin, Sebastián Vallejo Vera, and Ali Khaledi-Nasab. Depolarization of echo chambers by random dynamical nudge. *Scientific Reports*, 12(1):9234, 2022.
- [88] Elizabeth Dubois and Grant Blank. The echo chamber is overstated: the moderating effect of political interest and diverse media. *Information, communication & society*, 21(5):729–745, 2018.
- [89] Jaume Ojer, Michele Starnini, and Romualdo Pastor-Satorras. Modeling explosive opinion depolarization in interdependent topics. *arXiv preprint arXiv:2212.07879*, 2022.
- [90] Silvia Milano, Mariarosaria Taddeo, and Luciano Floridi. Recommender systems and their ethical challenges. *Ai & Society*, 35:957–967, 2020.
- [91] Emil Noordeh, Roman Levin, Ruochen Jiang, and Harris Shadmany. Echo chambers in collaborative filtering based recommendation systems. *arXiv preprint arXiv:2011.03890*, 2020.
- [92] Joe Whittaker, Seán Looney, Alastair Reed, and Fabio Votta. Recommender systems and the amplification of extremist content. *Internet Policy Review*, 10(2):1–29, 2021.
- [93] Charles Evans and Atoosa Kasirzadeh. User tampering in reinforcement learning recommender systems. *arXiv preprint arXiv:2109.04083*, 2021.
- [94] Muhammad Haroon, Anshuman Chhabra, Xin Liu, Prasant Mohapatra, Zubair Shafiq, and Magdalena Wojcieszak. Youtube, the great radicalizer? auditing and mitigating ideological biases in youtube recommendations. *arXiv preprint arXiv:2203.10666*, 2022.

- [95] Marilena Hohmann, Karel Devriendt, and Michele Coscia. Quantifying ideological polarization on a network using generalized euclidean distance. *Science Advances*, 9(9):eabq2044, 2023.
- [96] Barry C. Arnold, N. Balakrishnan, and H. N. Nagaraja. *A First Course in Order Statistics*. Society for Industrial and Applied Mathematics, 2008.
- [97] Milton Abramowitz and Irene A. Stegun. *Handbook of Mathematical Functions with Formulas, Graphs, and Mathematical Tables*. Dover, New York, ninth dover printing, tenth gpo printing edition, 1964.
- [98] Markku Laakso and Rein Taagepera. “effective” number of parties: a measure with application to west europe. *Comparative political studies*, 12(1):3–27, 1979.